CHAPTER 1

To understand the biochemical mechanisms of the role of sarm1 in mitochondrial electron transport chain (ETC) activity

1.1 Introduction

1.1.1 The protein SARM1: the fifth member of the TLR adaptor protein

Innate immunity is the first line of defence against foreign pathogens. Microbial components, showing pathogen associated molecular patterns (PAMPs), are recognized by pattern recognition receptors (PRRs). Toll like receptors (TLRs) are a kind of PRRs, located in cell membranes, endosomes or lysosomes. TLRs have an extracellular portion for ligand recognition, a transmembrane domain and a cytoplasmic portion that contains a TIR domain. TLRs are expressed in many cell types, including monocytes, macrophages, dendritic cells, T and B cells, epithelial and endothelial cells. 13 members of TLR family exist in mammals. Different TLR recognizes different PAMP. TLR2, TLR4, TLR5 and TLR11 are found in the cell surface and TLR3, TLR7, TLR8 and TLR9 are found in intracellular endosomes. They recognize PAMPs, including lipids (TLR2 and TLR4), proteins (TLR5 and TLR11) and nucleic acids (TLR3, TLR7, TLR8 and TLR9). After sensing the ligand, TLRs dimerization occurs which brings together their TIR domains to recruit the adaptor proteins. TLR signalling relies on five adaptor proteins, which are MyD88 (myeloid differentiation primary response gene 88), Mal (MyD88 adaptor like protein), TRIF (TIR domain containing adaptor protein inducing IFN-β), TRAM (TRIF related adaptor molecule) and SARM1 (Sterile alpha and TIR motif-containing 1 protein), who all possess TIR domain. These adaptors bridge between TLRs and downstream molecules, and lead to the activation of cytokines and regulation of adaptive immunity (Belinda et al., 2008; Carty et al., 2006; Fekonja et al., 2012; Kenny and O'Neill, 2008). TLRs initiate immune defence via MyD88 or TRIF dependent signalling pathways. MyD88 is an adaptor protein, which is used by all TLRs except of TLR3. MyD88 requires MAL to bridge with TLRs. MyD88 mediates MAPKs activation (Peng et al., 2010; Piao et al., 2009; Poole and Weis, 2014; Sheedy and O'Neill, 2007; Zhou et al., 2013). TRIF is an adaptor protein which uses TRAM as a bridging adaptor between its TIR domain and TLR. But unlike other 4 TLR adaptors, SARM1 acts as a negative regulator of the immune response (Belinda et al., 2008; Carty et al., 2006; Fornarino et al., 2011). It was found that SARM1 interacts with TRIF to inhibit TRIF dependent TLRs signalling. An increased SARM1 expression competes with TRIF for association with TLR4, which leads to inhibition of TLR4-TRIF association. SARM1 also negatively regulate MAPK phosphorylation

(Fig. 2) (Jenkins and Mansell, 2010; McGettrick and O'Neill, 2004; Mukherjee et al., 2013; O'Neill et al., 2003).

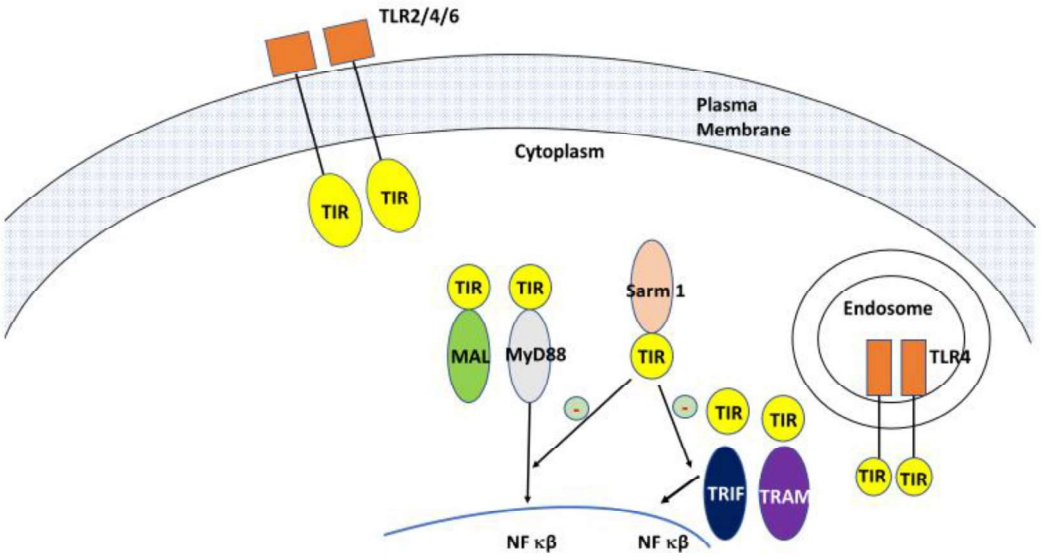

Fig. 2. TLR signalling involves a family of five adaptor proteins

Determination of structure and potential function of the individual domains of SARM1 is important to find its mode of action. SARM1 is a multidomain protein, containing an N terminal ARM domain, two central SAM domains and a C terminal TIR domain (Fig. 3) (Gong et al., 2016). Generally, proteins containing ARM domain act to regulate cytoskeleton, transport proteins between the cytosol and nucleus, control gene expression etc whereas, proteins containing SAM domain play diversified roles in transcription, translation, apoptosis etc (Panneerselvam and Ding, 2015).

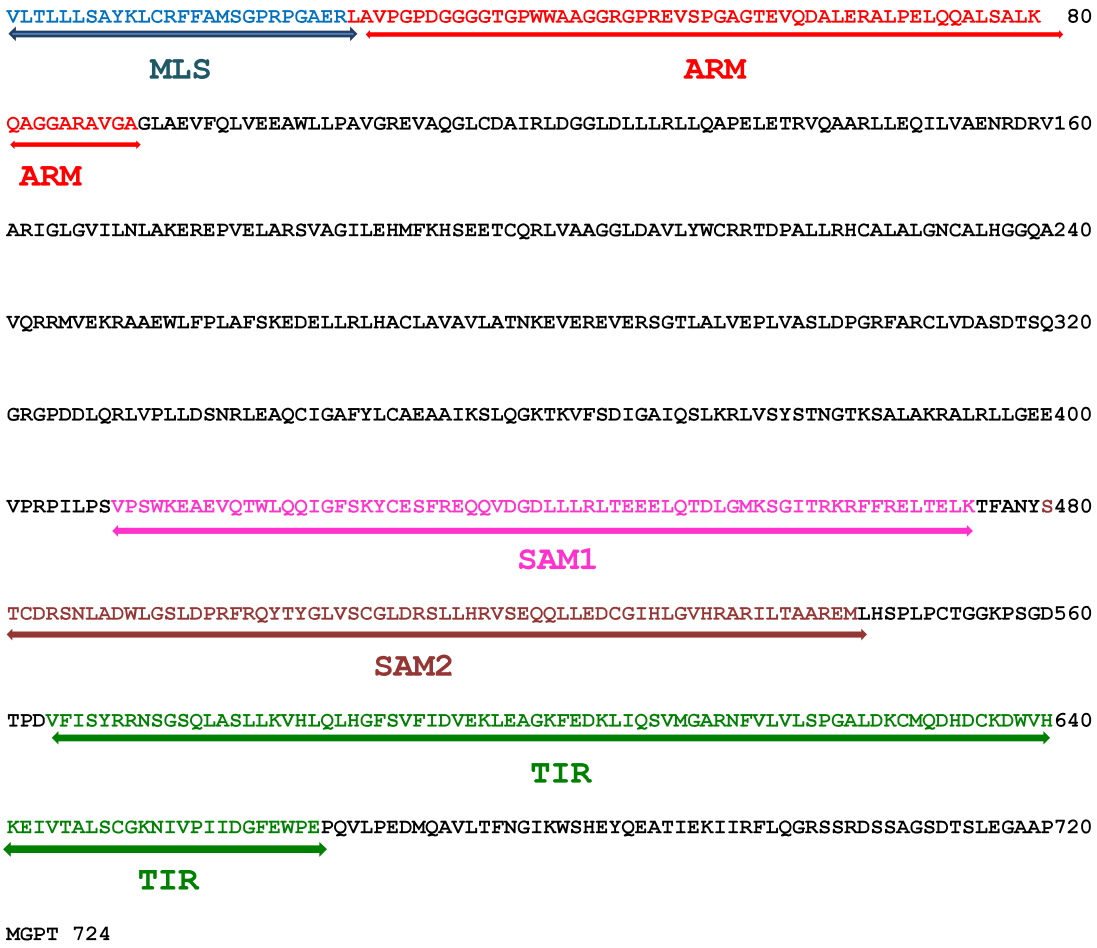

Fig. 3. Protein sequence of SARM1 indicating its functional domains; MLS (Mitochondrial localization signal), ARM (Armadillo), SAM1 and SAM2 (Sterile α motif), TIR (Toll/interleukin-1 receptor)

SARM1 lacking the HEAT/Armadillo repeats was not able to localize to mitochondria but was instead distributed in the cytoplasm. In contrast, SARM1, consisting of only the TIR domain, localized throughout the cytoplasm and nuclei (Kim et al., 2007). It was found that SARM1 experiences SAM dependent multimerization and that SARM1 needs its SAM domains intact to mediate axon degeneration. SARM1 lacking TIR domain disrupt SARM1 function but do not disrupt SARM1 multimerization (Gerdts et al., 2013). Indeed, SARM1 requires multimerization of TIR domain to induce axon degeneration. SARM1 mutant containing SAM and TIR domains but lacking N-terminal 408 a-a mediates axon degeneration even in the absence of injury. So, it was stated that N terminus of SARM1 is a negative regulator of SARM1 mediated neurodegeneration. It was speculated that in an axon, SARM1 exists in an auto inhibited state, which is post

translationally activated upon injury (Josiah Gerdts et al., 2013) and the N terminal ARM domain of SARM1 plays this autoinhibitory role, as SARM1 without ARM domain is constitutively active (Yang et al., 2015). It has been also observed that the proapoptotic function of SARM1 resides within the SAM and TIR domains (Panneerselvam et al., 2013). A physical interaction was also identified between the auto-inhibitory N-terminus and the TIR domain of SARM1, which mediates auto inhibition (Summers et al., 2016). Although several studies indicate that SARM1 mitochondrial localization is important for neurodegeneration, SARM1 protein without its N-terminal part is fully capable of mediating the axotomy induced axon degeneration. So, the importance of mitochondrial localization is not yet fully understood (Summers et al., 2014). SARM1 by using its amino terminal ARM domain, translocates to the nucleus, reported in human embryonic kidney cells. Once in the nucleus, SARM1 interacts with other proteins through its SAM domains to mediate nuclear apoptotic events (Sethman and Hawiger, 2013).

However, currently an insufficient structural detail of SARM1 protein is available. In a very recent work, SARM1 is hypothesized to be assembled into an octameric ring (Sporny et al., 2019). An electron microscopy analysis revealed octameric ring of both SARM1 and an isolated SAM domain of it. Crystal structure of SAM was shown to form a closed octameric ring in the crystal lattice. Interactions of SAM rings are mediated by complementing hydrophobic grooves and electrostatic charges between the neighbouring protomers (Sporny et al., 2019).

1.1.2 TIR domain of SARM1 and NADase activity

It has been determined that TIR domain of SARM1 induces NAD^+ loss and subsequent neurodegeneration, and this functional role is conserved from *C.elegans* to humans (Summers et al., 2016). After the neuronal injury or trauma, SARM1 has been reported to start breaking down of NAD^+, by dimerizing its TIR domain. SARM1 induced axon degeneration could be counteracted by increased NAD^+ synthesis (Gerdts et al., 2015). The TIR domain of SARM1 has its intrinsic NADase activity and cleaves NAD^+ into ADP-ribose (ADPR), cyclic ADPR and nicotinamide (Fig. 4). NAD^+ is required for many redox reactions (Essuman et al., 2017). The crystal structures of ribose and $NADP^+$ complexes of SARM1 and plant NLR RUN1 TIR domains show a conserved substrate binding site (Wan et al., 2019). Hence, TIR domains mediated NAD^+ cleavage could be considered as a conserved feature of

animal and plant cell death signalling pathways (Horsefield et al., 2019). In fact, a putative catalytic glutamic acid is conserved in both mammalian SARM1 NADase and bacterial TIR NADase (Wan et al., 2019). Animal SARM1 is closely related to bacterial TIR-domain containing proteins (Tcps) than other members of the TLR adaptor. This may suggest the common origin for these proteins and explain the inhibitory function of SARM1 in both bacteria and mammalian cells (Patterson and Werling, 2013).

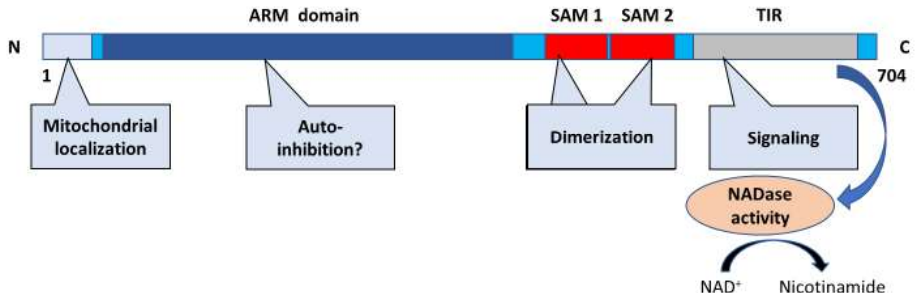

Fig. 4. TIR domain of SARM1 has NADase activity that cleaves NAD^+ into nicotinamide

Nicotinamide Riboside is a precursor of nicotinamide adenine dinucleotide that is converted to nicotinamide mononucleotide by specific enzymes, like nicotinamide riboside kinases, Nrk1 and Nrk2 (Fletcher et al., 2017). After the trauma or injury in neuron, SARM1 starts breaking down of NAD^+, by dimerizing its TIR domain. SARM1 induced axon degeneration could be counteracted by increased NAD^+ synthesis (Gerdts et al., 2015). NAD^+ precursors nicotinamide riboside (NR) is a promising drug candidates in view of their safety and efficiency in preclinical trials and natural existence in the human body (Fang, 2019). However recent data suggests that newly identified NAD^+ precursor, nicotinamide riboside (NR) may be the only vitamin precursor which supports neuronal NAD^+ synthesis (Bogan and Brenner, 2008).

1.1.3 Regulation of programmed axonal degeneration by SARM1

Axonal degeneration is an essential developmental event that proceeds through the selective destruction of axons (Schuldiner and Yaron, 2015). Axonal degeneration represents a feature of neurodegeneration and also occurs as a consequence of aging, constituting an important contributor to neuronal dysfunction (Neukomm and Freeman, 2014). Recent evidences indicate that degeneration of axon

is an early event in neurodegeneration, taking place prior to neuronal cell death (Adalbert and Coleman, 2013; Deckwerth and Johnson, 1994). Although, the actual molecular and cellular pathways through which degeneration of axon occurs is not yet known properly, key contributing factors have been identified in the last decade and important findings have contributed to determine the mechanisms involved. Interesting clues have been found by studying Wallerian degeneration (WD), that correspond to isolated axon degeneration after their mechanical transection (Mack et al., 2001). Wallerian degeneration is a form of programmed cell death that promotes breakdown of axon in injury and disease (Gerdts et al., 2016). This phenomenon was first described by Waller (Waller, 1843). He observed that cutting an axon away from its cell body was followed by a stereotyped blebbing, beading and fragmentation of the severed axon eventually (Fig. 5). The axon fragments were then removed by absorption. After axonal injury there was an eventual axonal fragmentation, together which is now described as Wallerian degeneration (Coleman, 2005). It was assumed that Wallerian degeneration occurred due to the severed starved axon, as it was not connected to a singular nutrient source, the cell body ('soma') any more (Lubińska, 1977). However, this phenomenon was suspected to have correlation with various neurological diseases, as it was hypothesized by Waller that similar alteration events of nerve fibres could be seen, particularly during paralysis (Waller, 1843). To determine which kind of mutation was able to block severed axons from degenerating, several generations of backcrossing was done and a mutation was found that acted in a dominant fashion (Perry et al., 1990). This mutation in the mice strain resulted from a tandem triplication (Coleman et al., 1998) and was termed as slow Wallerian degeneration (Wld^s) (Perry et al., 1990). This mutation caused the over expression of Wld^s, a novel chimeric fusion protein. First, 70 amino acids of this protein was ubiquitin conjugation factor E4B (ube4B) which was linked to the full length Nmnat 1, a NAD biosynthetic enzyme by an 18 amino acid linker from the 5' untranslated region (UTR) of Nmnat 1 (Conforti et al., 2000; Mack et al., 2001). Severed axons were protected in Wld^s cells in a dose-dependent manner (Mack et al., 2001).

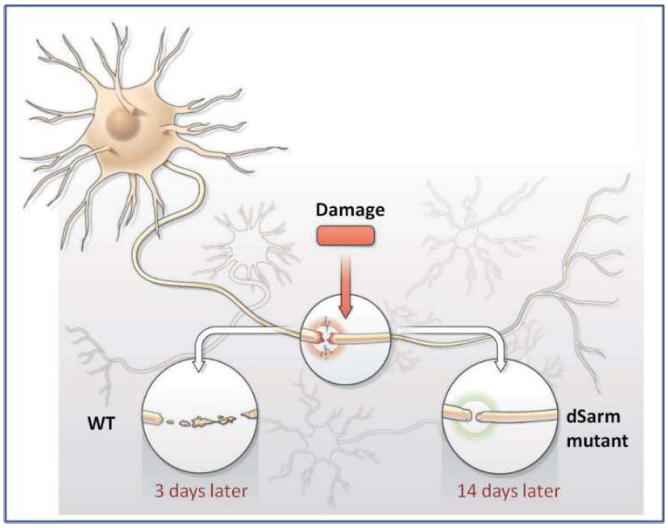

Fig. 5. Wallerian degeneration: After an axonal lesion, the segment distal to the cut undergoes fragmentation before it entirely disintegrates within three days. Loss of dSarm or overexpression of Wld^s in neurons keeps the distal axon intact even 14 days after the lesion. Adapted from Yu et al (Yu and Luo, 2012)

A Drosophila homolog of human SARM1 protein, dSarm was found to be the first mutant whose inhibition of axon degeneration was comparable to that of Wld^s protection. Using a forward genetic screen, Osterloh et al. discovered this mutation (Jeannette M. Osterloh et al., 2012). In this screening technique, animals with randomly generated mutations were screened for the desired phenotype, and pertinent genes were identified only after such phenotypes were identified. As the fly dSarm mutation is lethal, they created mosaic animals, in which dSarm gene was lost only in olfactory receptor neurons. When the neuronal cell bodies were removed from the brain, the cleaved axons remained intact for one month, which opposed to the severed wild type axons, which were degenerated and completely cleared within a week. Interestingly, the mechanism of Wallerian degeneration, shows morphological similarities with axon degeneration during axon pruning (normal brain development) and neurodegenerative diseases (Osterloh et al., 2012; Yu and Luo, 2012). Wallerian degeneration is distinct from apoptosis, because potent genetic or molecular inhibitors of apoptosis cannot block axonal fragmentation. Osterloh et al. identified three lines, l(3)896, l(3)4621, and l(3)4705 who were homozygous mutants (Jeannette M. Osterloh et al., 2012). Each dSarm allele contained a premature stop codon in open reading frame of dSarm and it was stated that l (3)896, l (3)4621, and l (3)4705 are loss of function alleles of dSarm. The Wallerian degeneration was also assayed in the null mutants of mouse SARM1. 5-day cultures of wild type, *Sarm1*$^{-/-}$ and Wld^s mice

superior cervical ganglia (SCG) were chosen, severed the axon and checked axonal integrity over the next week. Surprisingly, *Sarm1*$^{-/-}$ and Wld^{s} axons exhibited the protection from degeneration up to 72 hours after axotomy, whereas wild type explants degenerated within 8 hours. This strong protection was also noticed in cultured *Sarm1*$^{-/-}$ cortical neuron axons and dorsal root ganglia (DRG). It was also found that *Sarm1*$^{-/-}$ DRG neurons were not protected from nerve growth factor deficiencies, which suggests that SARM1 protection is unique for injury induced axonal death. To determine the requirement of SARM1 for Wallerian degeneration *in vivo*, sciatic nerve lesions were made in the right hind limb of *Sarm1*$^{-/-}$ mice and control. In the case of control mice, dramatic breakdown of axon and myelin sheath were found within 3 days of injury, whereas, in *Sarm1*$^{-/-}$ mice, 61.2% of lesioned axons were protected from degeneration after 14 days of their injury (Jeannette M. Osterloh et al., 2012).

Neuronal injury even results in reduction in glycolysis and respiration rate contributing to the reduced ATP supply. This is ameliorated by Wld^{s} protein as it is associated with maintenance of mitochondrial respiration and glycolysis. During the Wallerian degeneration, both mitochondrial respiration and glycolysis decline. Wld^{s} partially rescue their declination rate. Wld^{s} converts NMN and ATP to NAD and PPi through its NMNAT activity and both glycolysis and mitochondrial respiration requires NAD. However, SARM1 mutation (*Sarm1*$^{-/-}$) could also reduce the decline in glycolysis and respiration in a similar fashion, like Wld^{s} to delay Wallerian degeneration (Godzik and Coleman, 2015).

Axons depend on the constant supply of ATP to maintain axonal transport and release neurotransmitters. Failure to generate ATP results in severe axon damage (Godzik and Coleman, 2015). In damaged axons, SARM1 is required for the MAPK cascade activation and this pathway leads to the ATP depletion (Yang et al., 2015). It was proposed that although MAPK signalling is needed to activate SARM1 upon injury, but once SARM1 is active, then MAPK signalling is not essential for SARM1 dependent NAD^{+} depletion and axon degeneration (Walker et al., 2017).

1.1.4 SARM1 in the mitochondria

Transmission electron microscopy confirmed that the first 27 amino acids of SARM1 are responsible for the mitochondrial localization in HEK-293 cells (Mink et al., 2001). Preliminary *in vitro* work showed SARM1/GFP to be localized in

mitochondria after the overexpression in neuronal cultures, indicating that mitochondrial localization might be an artefact of SARM1 overexpression (Chuang and Bargmann, 2005). The mitochondria targeting signal sequence of SARM1 contains 27 amino acids, which are hydrophobic and polybasic, binds to lipid and mitochondria. An arginine residue resides in the 14th position of the sequence has the most potent ability to target mitochondria. This arginine either interacts with mitochondria import machinery or directly with the negatively charged head groups of phospholipid bilayer of mitochondrial membrane (Panneerselvam et al., 2012).

It was reported that in the mitochondria, SARM1 interacts with ATP synthase both *in vitro* and *in vivo*. In many studies, alteration in ATP synthase expression or function has been correlated with the ROS generation in mitochondria (Comelli et al., 1998; Natera-Naranjo et al., 2012). Although suppression of ATP synthase activity via SARM1 was not observed in La Crosse virus (LACV) induced neuronal death, but interaction of SARM1 with ATP synthase may affect ATP synthase function and influence ROS generation (Mukherjee et al., 2013). This was the first *in vivo* studies indicating SARM1 may play a role in mitochondrial ROS generating machinery by ETC complex regulation.

1.1.5 Role of ETC complex proteins in neurodegeneration

The electron transport chain is a mitochondrial pathway in which electrons move from NADH to reduce molecular oxygen (Kumari, 2017). The respiratory chain of mammalian mitochondria contains more than 20 carriers of electrons that are grouped into several multi-polypeptide complexes. Among them, three (I, III and IV) function as oxidation–reduction-driven proton pumps (Nicholls and Ferguson, 2002).

Dysfunctions of ETC complex proteins are responsible for many neurodegenerative diseases including Parkinson's disease (PD), Alzheimer's disease (AD) and Huntington's disease (HD). Structurally and functionally damaged mitochondria do not participate in sufficient ATP generation and are more prone to produce proapoptotic factors and reactive oxygen species (ROS), and these can mediate several mitochondrial disorders, including neurodegenerative diseases (Hroudová et al., 2014). The first evidence of mitochondrial involvement in pathogenesis of neurodegenerative process was reported when deficiency of complex I was detected in substantia nigra of patients with Parkinson's disease (PD) (Parker et al., 1989; Schapira et al., 1990). Again, strong evidences were also found for ETC

deficiencies: complexes II and III in Huntington's disease (HD) and complex I and cytochrome oxidase (complex IV, COX) in AD (Morán et al., 2012). It has been reported that alterations of the expression of mitochondrial and nuclear genes, encoding COX and complex I enzymes, promote damage in oxidative metabolism in AD (Aksenov et al., 1999). In AD brain specimens, downregulation of mitochondrial complex I genes was found (Manczak et al., 2004). Studies showed reduction of complex I activity (Chandrasekaran et al., 1996; Parker et al., 1989) and decreased gene expression of ND4 subunit of complex I in AD brains (Fukuyama et al., 1996). In AD brains, differential expression of mitochondrial genes encoding COX, complex I and complex V was determined (Manczak et al., 2004). Expressions of mitochondrial encoded COX I and nuclear encoded COX IV subunit were found in hippocampi of AD patients (Nagy et al., 1999). Altered proportions of subunits of COX, COX II, and COX IV mRNAs were found in the AD brains. Reduction in *ND4* and *ND15* mRNAs (encoding subunits of complex I) was found in AD patients. Alteration of these genes encoding parts of complex I and COX may contribute to damaged oxidative metabolism in AD patients (Aksenov et al., 1999). ETC activities of human lymphocytes were evaluated in AD patients and decline of complex III and COX activity was observed, along with increased complexes II and IV activities; this might be a compensatory mechanism to supply the energy (Feldhaus et al., 2011; Valla et al., 2006).

1.1.6 Concluding remarks

Taken together, these studies suggest that SARM1 plays a crucial role in programmed axonal degeneration. During neuronal stress, it translocates to the mitochondria and plays a role in mitochondrial ROS generation via interaction with ATP synthase. However, whether SARM1 regulates ETC complexes and how this correlates with subsequent neurodegeneration remains to be fully understood.

1.2 Materials and Method

1.2.1 *In silico* analysis

1.2.1.1 Retrieving the protein sequences

All sequences of proteins and particular domains chosen for analysis were obtained from protein database of National Center for Biotechnology Information

(NCBI). The isoforms whose sequences are closest to the consensus sequence were chosen. Non-redundant database was selected for searching relevant sequences.

1.2.1.2 Multiple sequence alignment

Multiple sequence alignment (Corpet, 1988) was performed *from* retrieved sequences. Multalin was used for this purpose. The sequences to be compared were pasted in the analysis window in fasta format. The output was obtained as an image file in jpg format.

1.2.1.3 Secondary structure prediction

CFSSP (Chou and Fasman Secondary Structure Prediction) server (Kumar, 2013) was used for the prediction of secondary structures of polypeptide chains. This is an empirical method based on the relative frequencies of amino acids present in alpha helices or beta sheets. The sequences to be compared were pasted in the analysis window in fasta format. The output was obtained as an image file in jpg format.

1.2.1.4 Homology modelling

Computational techniques such as homology modelling was chosen for the prediction of tertiary structures of proteins. 3-D structures of different domains of proteins were made by using The Phyre 2 (Protein Homology/analogY Recognition Engine) web portal (Kelley et al., 2015). Structures were visualized using RasMol tool (Sayle and Milner-White, 1995). The sequences to be compared were pasted in the analysis window in fasta format. The output was obtained as an image file in jpg format.

1.2.1.5 Comparison of protein structures

The structural refinement, comparison via superimposition was performed using UCSF Chimera 1.11.2 (Pettersen et al., 2004). RMSD values are listed in Table 6.

1.2.1.6 Prediction of binding site

Nucleotide binding sites on a protein or protein domain were predicted using proNA tool within the PredictProtein online software platform (Qiu et al., 2019). The sequences to be compared were pasted in the analysis window in fasta format. The output was obtained as an image file in jpg format.

1.2.1.7 Prediction of nuclear export signal (NES)

Nuclear export signal on a protein domain was predicted using NetNES 1.1 online server (la Cour et al., 2004). The sequences to be compared were pasted in the analysis window in fasta format. The output was obtained as an image file in jpg format.

1.2.2 *In vitro* studies

1.2.2.1 Generation of deletion mutants

Conventional molecular biological techniques (Sambrook et al., 1989) were used to generate the following expression constructs: C-terminal Flag-tagged SARM1 and SARM1 deletion mutants (Fig. 6). Primer sequences used in this technique are listed in Table 1.

Table 1. Sequences of primers used in this study

Domains	Sequences (size)
ΔN (R)	5'-TAATTACTCGAGGGTTGGACCCATGGGTGC-3' (30 mer)
ΔN (L)	5'-GGCGTAGAATTCATGGTAGAGAAGCGCGCA-3' (30 mer)
SAM1(R)	5'-CGCTCACTCGAGATAGTTGGCGAAGGTCTT-3' (30 mer)
SAM1(L)	5'-GGCGTAGAATTCATGGTAGAGAAGCGCGCA-3' (30 mer)
SAM2 (R)	5'-TAATTACTCGAGCATTTCTCTGGCCGCCGT-3' (30 mer)
SAM2 (L)	5'-ATTTAAGAATTCTCTACGTGCGACCGCAGC-3' (30 mer)
SAM (R)	5'-TAATTACTCGAGCATTTCTCTGGCCGCCGT-3' (30 mer)
SAM (L)	5'-GGCGTAGAATTCATGGTAGAGAAGCGCGCA -3' (30 mer)
TIR (R)	5'-TAATTACTCGAGCTCAGGCCACTCGAAGCC-3' (30 mer)
TIR (L)	5'-GGCTAAGAATTCATGCTACACTCCCCGCTG-3' (30 mer)
N-TERMINAL (R)	5'-AAATTTGAATTCGCCACCGCCCCCATCTGG-3' (30 mer)
N-TERMINAL (L)	5'-GCCTAAGAATTCATGGTCCTGACGCTGCTT-3' (30 mer)

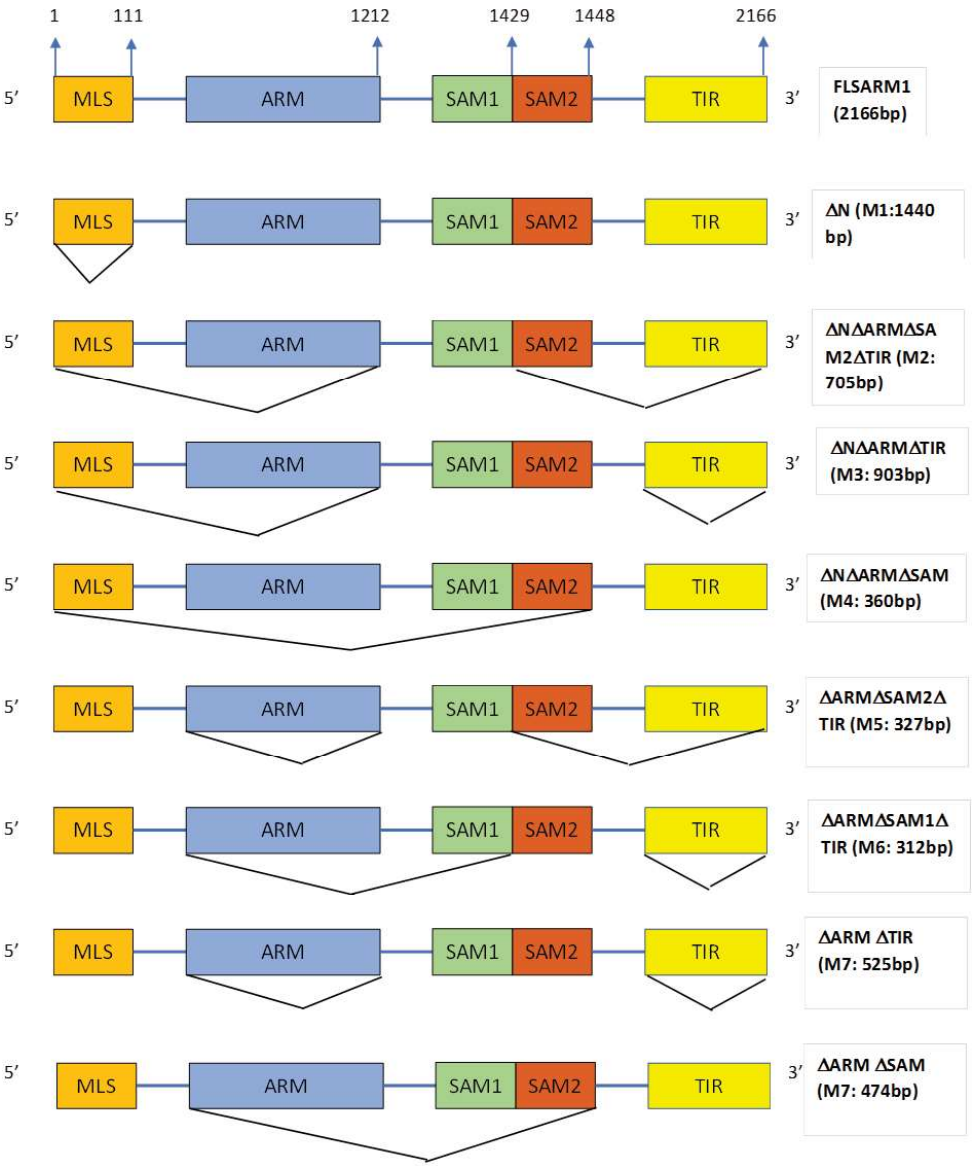

Fig. 6. Deletion mutants of SARM1 generated

Primer 3 (v. 0.4.0) web site was chosen to design all primers (Koressaar and Remm, 2007; Untergasser et al., 2012). All sequences of nucleic acids chosen for primer designing were obtained from nucleotide database of National Center for Biotechnology Information (NCBI). Primers were used to amplify the ORF of human SARM1 gene from full length human SARM1 gene, inserted in pCMV6 vector by standard PCR method (vide Section 1.2.2.4). Amplified gene segments of different mutants of SARM1 were cloned into the EcoRI and XhoI sites of pCMV6 vector to generate the C-terminal FLAG tagged construct (Fig. 7). All expression constructs were sequenced to ensure that the fusion was in the correct reading frame and there were no additional mutations.

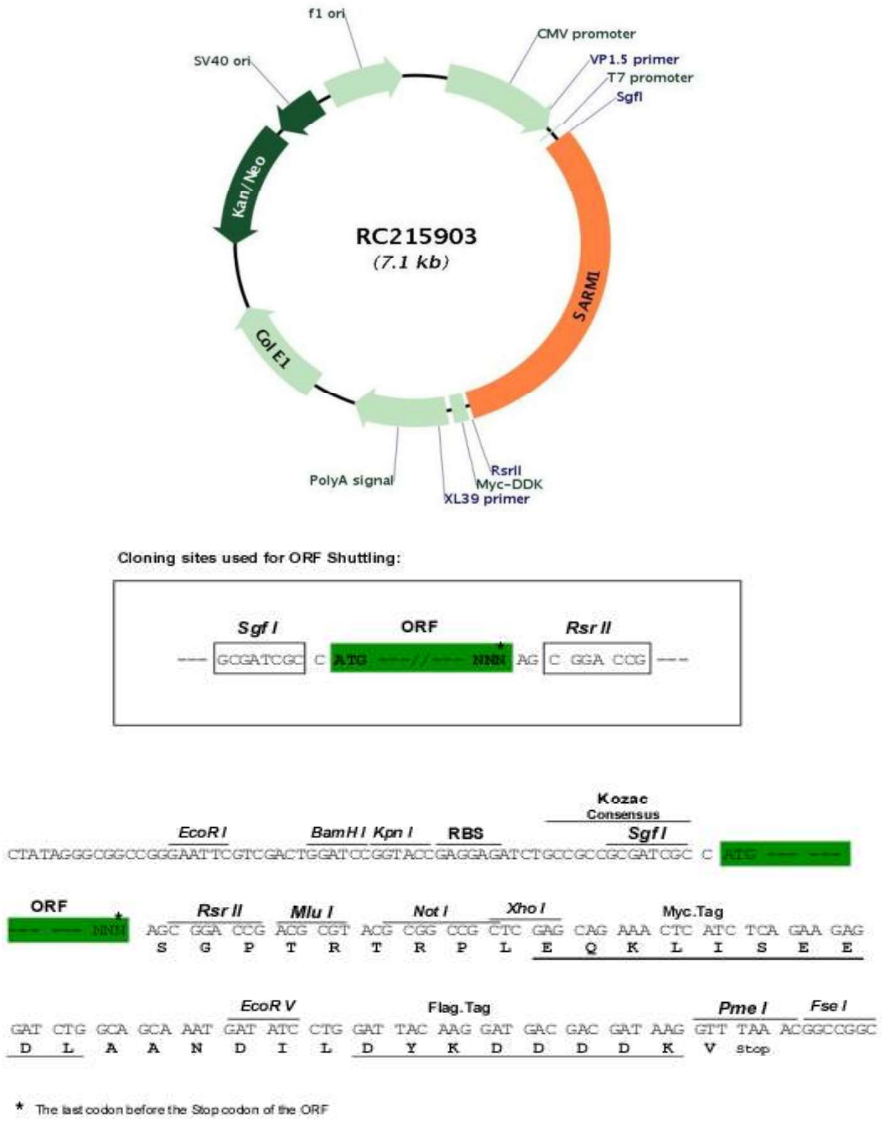

Fig. 7. Physical map of pCMV6 vector used for cloning SARM1 mutants

1.2.2.2 Isolation of plasmid DNA

Plasmid DNA was isolated from the bacterial organisms by the alkaline lysis method (Bimboim and Doly, 1979). Bacterial cultures grown freshly on Luria agar (LA) plates were used for the isolation of plasmid DNA. Briefly, a loopful of organisms, from a few prechecked colonies appearing in the plates, were used to inoculate 3 ml of Luria broth (LB) and incubated for 16-18 h at 37°C under mild shaking condition. Cells were then harvested at 8,000 x g for 10 min and resuspended by vortexing in 100 µl of solution I (vide Appendix) taken in a microcentrifuge tube. Following 10 min of incubation, 200 µl of freshly prepared solution II (vide Appendix) was added to the earlier suspension and mixed gently while keeping the

tube in an ice bath. Next 150 µl of ice-cold solution III (vide Appendix) was immediately added to it and mixed gently by mild agitation of the tube. Following incubation for 10 min at 4ºC, the mixture was centrifuged at 10,000 x g for 10 min at 4ºC and the clear supernatant (aqueous phase) was collected in a fresh tube. After sequential treatment of the aqueous phase with equal volumes of (a) buffer saturated phenol-chloroform (1:1) mixture and (b) chloroform alone, the plasmid DNA was precipitated by the addition of two volumes of ice cold absolute ethanol and collected by centrifugation (10,000 x g for 10 min at 4ºC). Next, the pelleted nucleic acid material was washed with 70% (vol./vol.) ethanol, air dried and reconstituted in 100 µl of Tris-EDTA (TE) buffer, pH 8.0 (vide Appendix).

Removal of RNA from isolated plasmid DNA material. Plasmid DNA, isolated following the protocol described above, was treated with a solution of DNase-free RNase (Sambrook et al., 1989) used at a final concentration of 20 µg/ml (wt./vol.) for 1 h at 37ºC. Next 3M sodium acetate solution, pH 5.2 was added to the plasmid DNA sample at a ratio of 1:9 (vol./vol.). The plasmid DNA was again treated with phenol-chloroform mixture and recovered through alcohol precipitation procedure as described earlier. The precipitated material was then washed with 70% (vol./vol.) ethanol, reconstituted in 50 µl of TE buffer (pH 8.0), and stored at 20ºC until used. Concentration of the plasmid DNA was estimated by measuring the OD value of the DNA solution at 260 nm. Alternatively, an approximate idea of the DNA concentration was obtained by visual examination of the electrophoresed DNA sample upon illumination in an UV transilluminator (Sigma).

1.2.2.3 Agarose gel electrophoresis

Preparation of the agarose gel. About 1.5 gm of agarose powder was taken in 100 ml of 1X TAE buffer (vide appendix) and heated on a boiling water bath. Molten agarose was then allowed to cool down to 60ºC and poured on the gel casting tray of 6 cm X 8 cm size.

Electrophoresis of DNA. DNA samples were subjected to agarose gel electrophoresis. For this, 0.5 µg of each DNA sample in 10 µl sterile nuclease free water was mixed with about 2 µl of DNA tracking dye solution (6X) and applied to each lane of the agarose gel. Electrophoresis was carried out on a horizontal unit, applying a constant voltage (initially 0.5 volt/ cm for 15 min and subsequently 2.5

volt/ cm), until the tracking dye reached a distance of about 1 cm away from the gel end (anode side).

Staining and visualization of DNA. Following electrophoresis, the gel was immersed in an aqueous solution (0.5 µg/ ml) of ethidium bromide and incubated for 20 min at room temperature. Next, the gel was rinsed with distilled water and viewed under UV light.

1.2.2.4 Polymerase Chain Reaction (PCR)

Amplification of target DNA was carried out by polymerase chain reaction using oligonucleotide primers specific for the target DNA sequence. Primer sequences used in this study are listed in Table 1. Primer 3 (v. 0.4.0) web site was chosen to design all primers (Koressaar and Remm, 2007; Untergasser et al., 2012). All sequences of nucleic acids chosen for primer designing were obtained from nucleotide database of National Center for Biotechnology Information (NCBI). Plasmid DNA preparations were utilised as the source of template DNA. The procedure for the preparation of plasmid DNA has been described earlier (vide Section 1.2.2.2).

PCR experiment for amplification of the target DNA was carried out in a thermal cycler (Biorad) using polypropylene tubes (Tarson, India) of 200 µl capacity, the final volume of the reaction mixture being 50 µl. Each 50 µl reaction mixture contained 1X Go Taq Green master mix, 0.5 µM of each primer and 100 ng of template DNA. The reaction mixture was subjected to amplification of 30-35 cycles, each of which consisted of three steps in the following order: denaturation of the template DNA at 94ºC for 30 s, annealing of the template DNA at temperatures between 56ºC to 64ºC (depending upon the melting temperature of the primers used) for 30 s and extension of the primers at 72ºC for 30 s. Before initiation of the first cycle, the reaction mixture was heated to 94ºC for 5 min to allow complete denaturation of the template. The PCR products, thus obtaind, were electrophoresed through 1% (wt./vol.) agarose gel to resolve the amplified products which were visualised under UV illumination after ethidium bromide staining (vide Section 1.2.2.3).

1.2.2.5 DNA extraction from agarose gel

DNA was extracted from agarose gels using a gel extraction kit, as per the manufacturer's instructions. Briefly, DNA was excised from agarose gel using a

sterile scalpel and collected in a clean microcentrifuge tube. The gel slice was weighed, dissolved in Binding buffer, CB (100 mg gel / 200 µl buffer) and incubated at 50ºC for 10 min until the gel slice got completely dissolved. The solution was then added to gel column by pipetting and centrifuged at 11,000 x g for 30 s at 4ºC. After the flow-through was discarded, 700 µl wash buffer, CW was added to the column, and centrifugation was done at 11,000 x g for 30 s at 4ºC. Another round of centrifugation was done to remove residual wash buffer CW. Finally, DNA was eluted in 20 µl of pre-heated Elution buffer C by centrifugation at 11,000 x g for 1 min at 4ºC. DNA concentration was measured by absorbance ratio of 260 and 280.

1.2.2.6 Recombinant DNA techniques

A. Restriction digestion of DNA

Restriction digestions of DNA samples were carried out using restriction enzymes (EcoRI and XhoI), digestion buffers and other reagents supplied by different manufacturers (vide Appendix). Methodologies used usually followed the user's manual provided by the respective manufacturers.

Table 2. Composition of a typical 50 µl of digestion mixture

Material		Amount
i)	DNA	1-5 µg
ii)	10 X reaction buffers (Specific buffers obtained from suppliers)	5µl
iii)	100 X aqueous solution of nuclease free BSA	0.5 µl (used only when recommended by the supplier of the restriction enzyme)
iv)	Restriction enzyme	0.5- 1 µl (5-10 U)
v)	Autoclaved water	Appropriate amount (µl) to make the final volume upto 50 µl

The digestion mixture was mixed well by gently tapping the tube and centrifuged at 5,000 x g for 30 s. The mixture was incubated at an optimum temperature (usually at 37ºC) and time interval (usually 3-4 h) as specified in the user's manual. The reaction was stopped by the addition of ethylenediaminetetraacetic acid (EDTA) (pH 8.0) at a final concentration of 10 mM or by heat inactivation at

68ºC for 10 min. Purification of the restriction digested DNA material was achieved by phenol-chloroform extraction and alcohol precipitation method as described earlier (vide Section 1.2.2.2).

B. Ligation of DNA

Ligation of DNA fragments (insertion of foreign DNA in a vector) was usually carried out by following the method as described below.

Table 3. Composition of a typical 20 µl of ligation mixture

Material		Amount
i)	Vector DNA (linearized by restriction digestion)	200 ng or 0.25 pmoles
ii)	10 X T4 DNA ligase buffer	2 µl or 2-fold molar excess of the DNA for cohesive end ligation
iii)	T4 DNA ligase	0.1-1 U
iv)	Autoclaved water	Appropriate amount (µl) to make the final volume upto 20 µl

The ligation reaction was carried out for 2-4 h (cohesive end ligation) at around 16ºC. Thereafter, the mixture was alcohol precipitated to isolate the DNA material.

C. Preparation of competent cells

Competent cells were prepared by following the methodology as discussed in a laboratory manual for molecular cloning (Sambrook et al., 1989). In this technique, competent cells were prepared by growing bacteria in LB (50-100 ml) at 37ºC (usually for 3-4 h) under shaking condition till the optical density at 600 nm (OD_{600}) [monitored by a photoelectric colorimeter] of the culture reached a value of about 0.5 to 0.6. Next, the culture was chilled on an ice bath and bacteria pelleted by centrifugation at 2,500 x g for 10 min at 4ºC. The cell pellet was resuspended in ice cold 100 mM $CaCl_2$ solution (1/4 th of the original volume of the culture) and chilled on an ice bath for 15 min. Cells were then pelleted by centrifugation at 2,500 x g for 10 min at 4ºC. Harvested bacterial pellet were resuspended in ice cold 100 mM $CaCl_2$ (1/20 th of the original volume) and kept on ice for about 2 h. Glycerol was then

added to the suspension drop by drop with gentle swirling to a final concentration of 15% (Vol./vol.). Competent cell suspension thus prepared was stored in aliquots of 0.5 ml at -70ºC.

D. Transformation of competent cells

Bacterial transformation by plasmid DNA was performed by, essentially, following the methodology as discussed in a laboratory manual for molecular cloning (Sambrook et al., 1989). For this, 200 µl of the competent cell suspension was mixed with the plasmid DNA sample (~ 5 µl containing 50 to 100 ng of DNA) and incubated on an ice bath for 30 min. Cells were then subjected to heat shock at 42ºC for 90 s and immediately chilled on ice for 2 min. Next, 1 ml of LB was added to the cell-DNA mixture and incubated at 37ºC under shaking condition for 1 h. Transformants were selected on LB agar supplemented with appropriate antibiotic(s).

1.2.3 Cell culture

A. Maintenance of SH-SY5Y cells

SH-SY5Y human neuroblastoma cells were procured from National Centre for Cell Science, Pune, India. SH-SY5Y cells were grown in culture dishes in DMEM-F12 medium, containing 10% (vol./vol.) fetal bovine serum (FBS) and 1% (vol./vol.) Penicillin-Streptomycin at 37ºC and 5% CO_2 in a humidified chamber. Cells were sub-cultured at 90-95% confluency. For sub-culturing cells, 0.25% trypsin-EDTA was added in the vials and allowed for 5 minutes at 37ºC. Cells were washed twice with 1X PBS and resuspended in culture medium. Resuspended cells were centrifuged at 3,000 rpm for 5 minutes at 4ºC. Supernatant was discarded and pellet was resuspended in culture medium that was added drop wise in cell culture dishes containing medium. Using the help of a haemocytometer, everyday cells were counted using a phase contrast microscope (Olympus, CKX53).

B. Maintenance of HEK293 cells

HEK293 cells were procured from National Centre for Cell Science, Pune, India. These cells were grown in culture dishes in Dulbecco's modified Eagle medium (DMEM), containing 10% (vol./vol.) fetal bovine serum (FBS) and 1% (vol./vol.) Penicillin-Streptomycin at 37ºC and 5% CO_2 in a humidified chamber. Cells were sub-cultured at 90-95% confluency. For sub-culturing cells, 0.25% trypsin-EDTA was added in the vials and allowed for 5 minutes at 37ºC. Cells were washed twice with 1X PBS and resuspended in culture medium. Resuspended cells were centrifuged at

3,000 rpm for 5 minutes at 4°C. Supernatant was discarded and pellet was resuspended in culture medium that was added drop wise in cell culture dishes containing medium. Using the help of a haemocytometer, everyday cells were counted using a phase contrast microscope (Olympus, CKX53).

C. Drug treatment in cell lines

Rotenone and Nimodipine (Structures shown in Fig. 8 A, B) were freshly prepared as 2 mM and 10 mM stock respectively in dimethyl sulfoxide (DMSO), Nicotinamide riboside (NR) and EGTA (structures shown in Fig. 8 C, D) were prepared freshly as 10 mM and 100 mM stock respectively in water before the start of the experiment, and subsequently dilutions were made in culture medium. Neuroblastoma cells were grown in culture medium containing these substances at a dose and time dependent manner, after which they were analysed. Control cells were incubated with the same concentration of DMSO (0.2%).

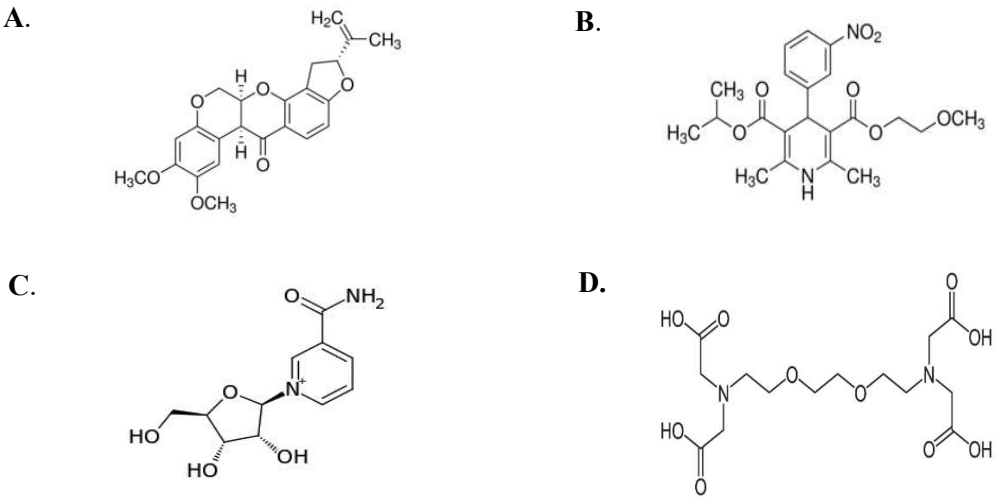

Fig. 8. Chemical structures of **(A)** Rotenone **(B)** Nimodipine **(C)** Nicotinamide Riboside (NR) and **(D)** EGTA

D. Analysis of cell growth and viability

Cells were cultured in 24 well plates and treated with media with or without drugs using 3 replicates per group per experiment. At specific time points, cells were incubated with 3-(4,5-Dimethylthiazol-2-yl)-2,5-Diphenyltetrazolium Bromide (MTT) at a concentration of 0.5 mg/ml for 3 h. The MTT solution was aspirated and DMSO was added to each well. The formazan concentration in each well was measured by taking absorbance at 540 nm using a cell plate reader (Synergy, BioTek).

Treated sample data were compared with control samples to determine percent cell death.

1.2.4 Real-Time PCR

A. RNA isolation

Total RNA was extracted from cells by using TRI reagent according to the manufacturer's instruction. Briefly, 1 ml of Trizol was added to the cells and allowed to stand for 10-15 min at room temperature. Next, 200 µl of chloroform was added, shaken vigorously for 15 s and allowed to stand for 15 min at room temperature. Following centrifugation at 12,000 x g for 15 min at 4ºC, the aqueous phase was separated in a new tube and 500 µl of isopropanol was mixed with it and allowed to stand for 10 min at room temperature. Next, the samples were centrifuged at 12,000 x g for 10 min at 4ºC, the supernatant was removed, and the RNA pellet thus obtained, was washed with 1 ml of 75% ethanol. The samples were vortexed and then centrifuged at 7,500 x g for 5 min at 4ºC. Finally, the RNA pellet was air dried for 10 min and resuspended in 30 µl of RNase free water. The RNA preparation was heated at 55ºC for 15 min to melt the secondary structures and immediately cooled on ice. The extracted RNA material was treated with 2 U of RNase-free-DNase and the total RNA, thus obtained, was subjected to reverse transcription experiments as described below.

B. cDNA synthesis

cDNA was prepared from RNA samples by reverse transcription PCR using cDNA synthesis kit according to the manufacturer's instruction. 1µg of RNA and 1X iScript RT supermix were taken to produce cDNA. cDNA synthesis reaction was as follows: Priming for 5 min at 25ºC, Reverse transcription for 20 min at 46ºC, RT inactivation for 1 min at 95ºC.

C. Real-Time PCR analysis

Amplification of the cDNA was carried out by polymerase chain reaction (PCR) using Q-PCR kit according to the manufacturer's instruction. Primer sequences used in this study are listed in Table 4. Primer 3 (v. 0.4.0) web site was chosen to design all primers (Koressaar and Remm, 2007; Untergasser et al., 2012). All sequences of nucleic acids chosen for primer designing were obtained from nucleotide database of National Center for Biotechnology Information (NCBI). PCR experiments

for amplification of the target DNA was carried out in a thermal cycler (Biorad) using polypropylene tubes of 200 µl capacity containing 10 µl of the reaction mixture. Each of the reaction mixture consisted of 1 µl of cDNA (obtained by reverse transcription experiments), 1 µl of each of the primer pair, 5 µl of 2X SYBR green dye and 3 µl of distilled water. Thermal cycling conditions were 95ºC for 3 min, followed by 40 cycles at 95ºC, 10 s, for denaturation, and 15 s at 60ºC for annealing and 15 s at 72ºC for extension. Data for each sample was calculated as the percent difference in CT values (delta CT=CT GAPDH-CT gene of interest). The data was plotted as mean percent GAPDH values for each gene of interest for each sample.

Table 4. Sequences of primers used in this study

Target genes	Sequences (size)
GAPDH (R)	5'-GCCTTCTCCATGGTGGTGAAGAC-3' (23 mer)
GAPDH (L)	5'-CCCATCACCATCTTCCAGGAGC-3' (22 mer)
Ndufv1 (R)	5'-ACCTTTCAGCCTCCAGTCATGG-3' (22 mer)
Ndufv1 (L)	5'-CACGACAGCACCCAAGAAAACC-3' (22 mer)
Ndufv2 (R)	5'-CCACTCCTTGGCCCTGGTTT-3' (20 mer)
Ndufv2 (L)	5'-GTGGAATGTTTAGGGGCCTGTGT-3' (23 mer)
Ndufs2 (R)	5'-TGCAGGAGCCCGATGTGA-3' (18 mer)
Ndufs2 (L)	5'-ACCCTGAACTTTGGGCCCC-3' (19 mer)
Cyc1 (R)	5'-GATGTAGCTGAGGTCAGGGGG-3' (21 mer)
Cyc1 (L)	5'-GGGAGATGTTCATGCGGCCA-3' (20 mer)
Cox5A (R)	5'-GCAGCATCAATGATTTTGGGCTC-3' (23 mer)
Cox5A (L)	5'-GTTTGATGCTCGCTGGGT-3' (18 mer)
Cox5B (R)	5'-TGGGGCACCAGCTTGTAATGG-3' (21 mer)
Cox5B (L)	5'-GGCTGCATCTGTGAAGAGGACAA-3' (23 mer)
Atp4A (R)	5'-GCGAGGAGTTGTCCACCTTGC-3' (21 mer)
Atp4A (L)	5'-GGCGACCTGGTGGAGATGAAA-3' (21 mer)
Atp4B (R)	5'-GTTGCTGGGGAGGAACTTGAC-3' (21 mer)
Atp4B (L)	5'-AACTGCTCAGGCCTGGCG-3' (18 mer)
Atp12A (R)	5'-CTGGGGCTCAGACTCCCC-3' (18 mer)
Atp12A (L)	5'-AGAGCAGCTGGTGGTGGG-3' (18 mer)
Sarm1 (R)	5'-GCTTGAACATGTGCTCCAAGATGCC-3' (25 mer)
Sarm1 (L)	5'-GAGCAGATCCTGGTGGCTGAGAA-3' (23 mer)
SirT1 (R)	5'-AAGTTGTCGGCCAGCGGT-3' (18 mer)
SirT1 (L)	5'-TGGGGAAGGAGACAATGGGC-3' (20 mer)
SirT3 (R)	5'-AGAATGGGAGTTCAAAAATGGCCT-3' (24 mer)
SirT3 (L)	5'-ATCAGCACACCCAGTGGCATT-3' (21 mer)
SirT4 (R)	5'-CGATCCAACGGCCTTTTGCTGA-3' (22 mer)
SirT4 (L)	5'-AGACGGTCCCACTGTGGG-3' (18 mer)
SirT5 (R)	5'-ACATTTCCATTTACTTGGGCCCCG-3' (24 mer)
SirT5 (L)	5'-GGACACAGCGCCTCTAGGAGAAAG-3' (24 mer)
SirT6 (R)	5'-ACTTGCCCTTGTCCGCGT-3' (18 mer)
SirT6 (L)	5'-GAAGCGGCCTCAACAAGGGAAA-3' (22 mer)
SirT7 (R)	5'-TGCTCCTCCCGCAACCTC-3' (18 mer)
SirT7 (L)	5'-TGCCGTGTGAGGCGGAAG-3' (18 mer)

1.2.5 Immunoblot experiments

Methodologies adopted for immunoblotting experiments are described below. Antisera used for this purpose are listed in Table 5.

A. Preparation of cell lysate

Whole cell lysates were prepared after lysing cells with M-PER Mammalian Protein Extraction Reagent supplemented with the Complete Protease Inhibitor Cocktails according to the manufacturer's manual. Cells were cultured for different time points in 6 well plates and were harvested at 1,200 x g for 5 min at 4ºC and pellets were resuspended in 200 µl M-PER mixed with 1X Protease inhibitor. Cells suspended in M-PER were allowed to lyse by keeping at 4ºC for 30 min, and repeated vortexing were done, then cells were centrifuged at 12,000 x g for 3 min at 4ºC, the supernatant was collected and kept at -20ºC.

B. Protein estimation

Protein contents of cell lysates/ cell fraction were determined using the Bradford reagent according to the manufacturer's protocol. Briefly, 5 µl of test sample was mixed with 495 µl of double distilled water and to it 500 µl of Bradford reagent was added. The optical density of the mixture was measured at 595 nm (Bradford, 1976). The optical density value of the blank (500 µl of water + 500 µl of Bradford reagent) was subtracted from the optical density of the test sample and the resulting value was compared with a standard curve (Fig. 9), generated with known concentrations of bovine serum albumin.

20 µg of protein were taken in Laemmli buffer, heated in a boiling water bath for about 5 min and thereafter, immediately placed on ice. Samples, thus prepared, were applied to individual lanes of SDS-polyacrylamide gel and subjected to electrophoresis as described below.

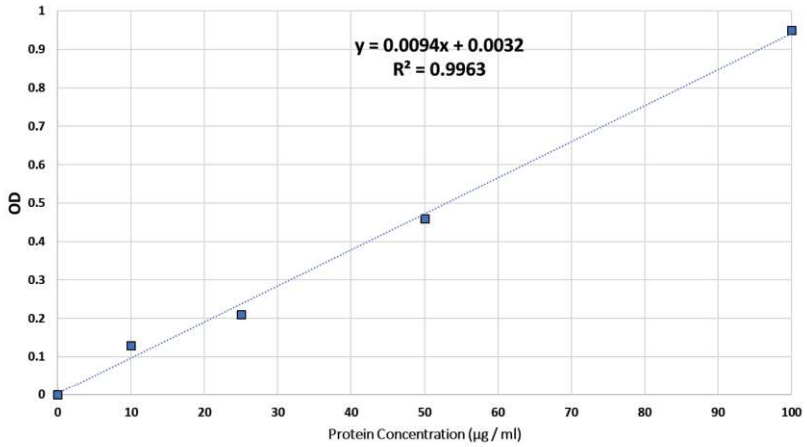

Fig. 9. Standard curve of BSA

C. Sodium dodecyl sulphate-polyacrylamide gel electrophoresis (SDS-PAGE)

Test samples were electrophoresed in SDS polyacrylamide gel by the method of (Laemmli, 1970). This technique consisted of the following steps:

Casting of gel slab. One mm gel was cast between two glass plates (10 cm X 10 cm). For this, about 9 ml of the gel mixture [containing 12.5% (wt./vol.) acrylamide, 0.33% (wt./vol.) N, N'-methylene-bis-acrylamide, 0.1% (wt./vol.) sodium dodecyl sulphate (SDS), 0.038% (wt./vol.) potassium persulphate, 0.06% (vol./vol.) of N,N,N',N'-tetramethyl ethylene (TEMED) in 1.5 M Tris-HCl buffer, pH 8.3] was used to prepare the separating gel which was overlaid with a few drops of water. After polymerization, the water layer at the top of the gel was removed and the stacking gel mixture [containing 4.5% (wt./vol.) of acrylamide, 0.12% (wt./vol.) of N, N'-methylene-bis-acrylamide, 0.1% (wt./vol.) of SDS, 0.03% (wt./vol.) of potassium persulphate, 0.1% (vol./vol.) of TEMED in 0.5M Tris-HCl buffer, pH 6.8] was applied on the top of the separating gel. A comb was then inserted into the stacking gel mixture and the gel was allowed to polymerise. Following polymerization of the stacking gel, the comb was removed and slots, thus formed, were washed with the electrode buffer, pH 8.3 (vide Appendix).

Electrophoresis. The test samples, prepared for SDS-PAGE, were electrophoresed onto a vertical acrylamide gel slab (9cm X 7cm) using a gel electrophoresis apparatus (Biorad) under a constant voltage (initially 60 volts was applied which was subsequently increased to 120 volts) at room temperature. Electrophoresis was continued until the tracking dye reached 1 cm above the bottom (anode end). For each electrophoresis run, one lane contained a mixture of pre stained marker proteins of

known molecular weights such as, triosephosphate isomerase (31.4 kDa), lactic dehydrogenase (37 kDa), ovalbumin (53.5 kDa), pyruvate kinase (81 kDa), fructose-6-P kinase (102 kDa) and β-galactosidase (126 kDa).

D. Electroblotting. Following electrophoresis, gels were taken out from glass plates and allowed to equilibrate with the blot buffer (vide Appendix) for about 10 min. Nitrocellulose membranes of suitable sizes were soaked in the same buffer for 10 min. Next, gels were transferred to thick absorbent pads pre-soaked with the blot buffer. Thereafter, pre-soaked nitrocellulose membrane (0.2 µm pore size) of appropriate sizes were placed over the gel, taking care not to trap any air bubbles in between the membranes and the gel. These were then overlaid with another set of thick absorbent pads to form a sandwich. This complete sandwich was then transferred to the transblot apparatus (Biorad), so that the nitrocellulose membrane faced towards the anode. Subsequently, the protein samples in the gel were electrophoretically transferred to the membrane strip at room temperature by applying a constant current of 170 mA for 1-2 h. Next, the blotted nitrocellulose paper was washed with 1X TBST (vide appendix) and kept for immunostaining. A portion of the blotted strip, which contained electrophoretically separated prestained marker proteins, was cut and kept at 4 ºC for a comparison with the bands generated following immunostaining of the test samples.

E. Immunostaining. Following electroblotting, membrane strips were placed in small plastic trays and treated with a solution of 10 mM Tris-HCl buffer (pH 7.4) and 100 mM NaCl containing 5% (wt./vol.) skimmed milk at 4ºC (for overnight) or 37ºC (for 2 h) to saturate the unbound sites. The membrane was then washed thrice with Tris buffered saline (TBS), pH 7.4 (vide Appendix) containing 0,05% (vol./vol.) Tween 20 (TBS-Tween 20). Next, the membrane was incubated with specific antibody (Table 5), for 2 h at room temperature or for overnight at 4ºC. After incubation and washing, the strips were incubated at room temperature for 2 h with diluted (1:10,000 dilution in TBS-5% skimmed milk) goat anti-mouse or anti-rabbit IgG Horse Radish Peroxidase (HRP) conjugate. Following washing bands were visualized using the enhanced chemiluminescence (ECL) solution. Levels of β-actin were used to normalize protein levels. The band intensity was quantified by ImageJ.

Table 5. List of primary and secondary antibodies used in this study

Protein to be detected	Primary antibody used and its dilution	Time of incubation	Secondary antibody used
β-actin	Anti- β-actin mouse monoclonal antibody (abcam) used at a dilution of 1:1000	*2h **overnight	Goat anti-mouse IgG H&L (HRP) preadsorbed (abcam) at 1/5000 dilution
Cox IV	Anti- COX4 mouse monoclonal antibody (Thermo) used at a dilution of 1:1000	*2h **overnight	Goat anti-mouse IgG H&L (HRP) preadsorbed (abcam) at 1/5000 dilution
Lamin	Anti- Lamin mouse monoclonal antibody (DSHB) used at a dilution of 1:100	*2h **overnight	Goat anti-mouse IgG H&L (HRP) preadsorbed (abcam) at 1/5000 dilution
SARM1	Anti- SARM1 rabbit polyclonal antibody (Cell Signaling) used at a dilution of 1:1000	*2h **overnight	Goat anti-rabbit IgG H&L (HRP) preadsorbed (abcam) at 1/5000 dilution
*Blocking with 5% skimmed milk for 30 min at room temperature. **Incubation with antibody for 2 h at room temperature or overnight at 4-degree C.			

1.2.6 Isolation of mitochondrial fraction

Mitochondria were isolated from them using Mitochondria Isolation Kit according to the manufacturer's instruction. Briefly, cells were harvested in a 2.0 ml microcentrifuge tube at 850 x g for 2 minutes. The supernatant was discarded. 800 µl of Mitochondria isolation Reagent A was added to the pellet. After a 5 s of vortexing, tube was kept in ice for 2 minutes. Then 10 µl of Mitochondria isolation Reagent B was added to the solution. After a 5 s of vortexing, tube was kept in ice for 5 minutes. Then 800 µl of Mitochondria isolation Reagent C was added to the solution. It was centrifuged at 700 x g for 10 minutes at 4^{o}C. The supernatant was transferred to a new tube and centrifuged at 12,000 x g for 15 minutes at 4^{o}C. The pellet contains the isolated mitochondria.

To isolate mitochondrial protein, mammalian protein extraction reagent (M-PER) was added directly to the isolated mitochondrial pellet which followed the same procedure of whole cell lysate preparation (vide Section 1.2.2.9 A).

1.2.7 Isolation of nuclear fraction

SH-SY5Y cells were cultured in 100 mm plates for different time span depending on the drug treatment. Cells were harvested in a 1.5 ml microcentrifuge tube at 850 x g for 2 minutes. The supernatant was discarded. 300 µl of Buffer A with Triton X 100 (vide Appendix) was added to the pellet and allowed to incubate for 5 minutes on ice. Then it was centrifuged at 2,000 x g for 5 minutes at 4ºC. The supernatant contains cytosol. 300 µl of Buffer A without Triton X 100 (vide Appendix) was added to the pellet and centrifuged at 2,000 x g for 5 min at 4ºC. The supernatant was discarded. 300 µl of Buffer B (vide appendix) was added to the pellet and allowed to incubate for 30 minutes on ice. Then it was centrifuged at 2,000 x g for 5 minutes at 4ºC. The supernatant was discarded. The pellet contains the isolated nucleus.

To isolate nuclear protein, 300 µl of Buffer A without Triton X 100 (vide Appendix) was added to the pellet directly to the isolated nuclear pellet. 4 X Laemmli buffer was added in it and boiled for 3 minutes and sonicated to isolate nuclear protein.

1.2.8 Immunocytochemistry

SH-SY5Y and HEK293 cells were cultured in 8-well chamber slides for different time span depending on the drug treatment. Cells were fixed with 2% formaldehyde and permeabilized by the treatment with PBST (0.1% Triton X-100 in PBS) for 5 min at 4ºC. After blocking for 1 h with 1% Normal donkey serum (NDS), cells were incubated with respective first antibodies, washed twice and the samples were incubated with Alexa Fluor 488 and 594 goat anti-mouse and rabbit IgG antibody. Then cells were labelled with DAPI in PBS for 5 min, washed for 10 min in PBS and mounted in fluoroshield mounting media onto microscopic slides. Cells were photographed under a fluorescent microscope (Leica Microsystems). For FITC, fluorescence was measured at λex=495 nm and λem=519 nm (Donkey Anti-Mouse secondary antibody) and λex=555 nm and λem=565 nm (Donkey Anti-Rabbit secondary antibody). In case of DAPI, fluorescence was measured at λex=359 nm and λem=461 nm.

1.2.9 Mitochondrial staining

A. Staining with Mitotracker green

SH-SY5Y cells were cultured in 8-well chamber slides for different time span depending on the drug treatment. To SH-SY5Y cells, Mitotracker green was added to achieve the final concentration of 100 nM and incubated for 20 min at 37ºC. Cells were photographed under a fluorescent microscope (Leica Microsystems). Fluorescence was measured at λ_{ex}=490 nm and λ_{em}=516 nm.

B. Staining with TMRM

HEK293 cells were cultured in 8-well chamber slides for different time span depending on the drug treatment. To HEK293 cells, TMRM was added to achieve the final concentration of 250 nM and incubated for 20 min at 37ºC. Cells were photographed under a fluorescent microscope (Leica Microsystems). Fluorescence was measured at λ_{ex}=546 nm and λ_{em}=552 nm.

1.2.10 Transfection of cells

A. Transfection of SH-SY5Y with FL-SARM1 and its deletion mutants

SH-SY5Y cells were cultured in 35 mm plate. Cells were transfected with 2.5 µg of DNA using Lipofectamine 2000 according to the manufacturer's instruction for 48 h. Briefly, 5.5 µl of Lipofectamine 2000 was mixed with 144.5 µl of OptiMem media in a polypropylene tube of 1.5 ml capacity. In another tube, 8 µl DNA (~ 2.5 µg) was mixed with 142 µl of OptiMem media. Then, the contents of both tubes were mixed and incubated for 5 minutes at RT. From that, 300 µl mixture was added in each 35 mm plate, containing 1.7 ml media.

B. Transfection of SH-SY5Y with SARM1 siRNA

SH-SY5Y cells were cultured in 24 well plate. Cells were transfected with 10 nM of SARM1 (ambion, life technologies) siRNA using Lipofectamine 2000 according to the manufacturer's instruction for 24 h and 48 h. Briefly, 3 µl of 10 µM SARM1 siRNA was mixed with 57 µl sterile nuclease free water in a polypropylene tube of 1.5 ml capacity. Then 200 µl OptiMem media was mixed with 50 µl of above solution. In another tube, 5 µl Lipofectamine 2000 was mixed with 245 µl of OptiMem media. Then, the contents of both tubes were mixed. From that, 100 µl mixture was added in each well of 24 well plate, containing 400 µl media.

Cells were also treated with a nontargeting siRNA (ambion, life technologies) with no known mammalian homology as a negative control. 0.5 µl of 50 µM negative control stock was mixed with 49.5 µl sterile nuclease free water in a polypropylene tubes of 1.5 ml capacity. In another tube, 1 µl Lipofectamine 2000 was mixed with 49 µl of OptiMem media. Then, the contents of both tubes were mixed. From that, 100 µl mixture was added in each well of 24 well plate, containing 400 µl media.

1.2.11 Measurement of intracellular NAD^+ level

SH-SY5Y cells were cultured in 100 mm plates for different time span depending on the drug treatment. Cells were prepared and assay was performed by using NAD/NADH assay kit according to the manufacturer's instruction. Cells were scrapped in 1X cold PBS and then centrifuged at 1,500 rpm for 5 minutes at RT. Pellet was resuspended in 1 ml cold 1X PBS. Cells were counted and centrifuged again. 5 X 10^6 cells were resuspended in 100 µl lysis buffer. Cells were incubated for 15 minutes at 37°C. Cell lysate was centrifuged at 1,500 rpm for 15 minutes and supernatant was used for the assay.

25 µl standard solution is kept in a standard well. Similarly, 25 µl of control and test samples are kept separately in sample wells. All standard, control and test samples are prepared in duplicate. 25 µl of NAD extraction solution was added into sample wells and incubated for 10-15 minutes at 37°C. 25 µl of NADH extraction solution was added into sample wells to neutralize NAD extracts. 75 µl of NADH reaction mixture was added into each well and incubated for 2 h at RT. Fluorescence was measured at λ_{ex}=540 nm and λ_{em}=590 nm using a cell plate reader (Synergy, Bio Tek).

1.3 Results

1.3.1 *In silico* analysis of SARM1

1.3.1.1 TIR domain of SARM1 is responsible for the opposite functional roles of *C.elegans* and human SARM1

Across phyla, SARM1 gene is highly conserved, since *Caenorhabditis elegans* and Drosophila SARM1 (tir-1 and dSarm, respectively) share more than 40% identity with human SARM1 (Mink et al., 2001). However, sequence variation of *C. elegans* SARM1 and SARM1 of other organisms is almost similar, although they have just opposite functional role (Akhouayri et al., 2011; Wang et al., 2013). In worms,

genetic ablation of *tir-1* or *tir-1* knockdown with RNAi resulted in increased susceptibility to death by bacterial and fungal infections (Couillault et al., 2004; Kurz et al., 2007; Liberati et al., 2004). On the other hand, SARM1 acts as a negative regulator of antimicrobial responses in Drosophila and shrimp unlike worms (Akhouayri et al., 2011; Wang et al., 2013). In mammals, SARM1 has been shown to negatively regulate the innate immune response (Carty et al., 2006; Peng et al., 2010; Yuan et al., 2010). In order to compare different domains of SARM1 such as SAM1, SAM2 and TIR between *Homo sapiens,* and *C. elegans*, polypeptide sequences of these two proteins were chosen for the computational analysis. Tertiary structures of these domains (Fig. 10 A-F) and their root-mean-square deviation (RMSD) value was predicted based on 3-D structures (Table 6).

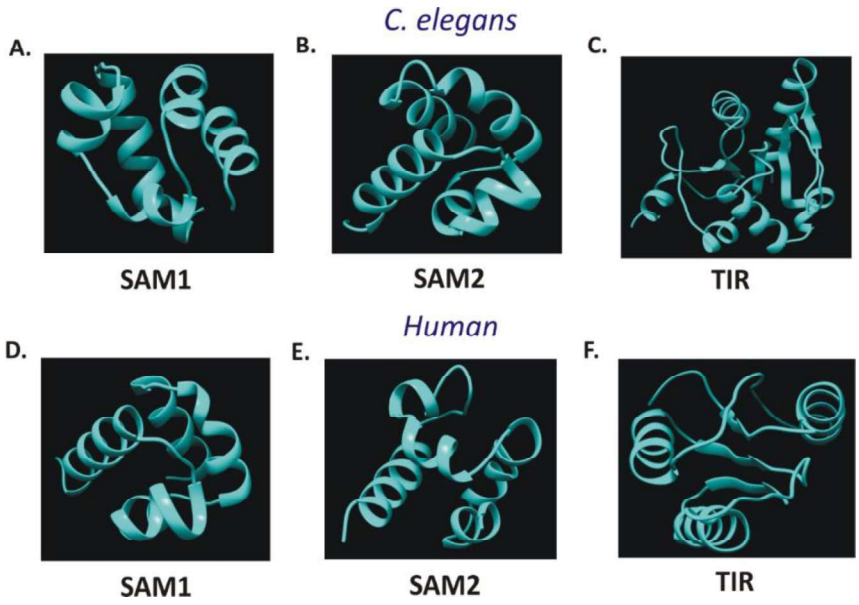

Fig. 10. Tertiary structure prediction of **(A)** SAM1 **(B)** SAM2 **(C)** TIR domain of *C.elegans* SARM1 and **(D)** SAM1, **(E)** SAM2 **(F)** TIR domain of *H.sapiens* SARM1

Table 6. Alignment results of three domains of *C.elegans* and human SARM1 protein

S. No	Complex name	RMSD Å
1.	*C. elegans* TIR-Human TIR	3.347
2.	*C. elegans* SAM1-Human SAM1	1.026
3.	*C. elegans* SAM2-Human SAM2	0.485

Smaller the RMSD value, closer two protein sequences are. A larger value represents them as dissimilar and zero value represents them as identical (Maiorov

and Crippen, 1994). The lowest RMSD values should be less than 2 Å (Oferkin et al., 2015). From our results, we predicted that SAM1 and SAM2 domains of *C. elegans* are very similar to SAM domains of human SARM1, as they have RMSD values 1.026 and 0.485 Å respectively. However, comparison of TIR domain of SARM1 from *C.elegans* and human showed a larger RMSD value (3.34 Å), indicating that TIR domain of these two organisms is dissimilar. These findings might explain the opposite functional role of the same protein in these two organisms implying that not SAM but TIR domain of SARM1 might be involved in the opposite functional role of this protein, the mechanism of which needs to be explored further.

1.3.1.2 Human SARM1 TIR is closer to bacterial TcpB TIR compared to other human adaptor TIRs

Although activity of SARM1 is dependent on the integrity of the protein's SAM and TIR domains, insufficient structural information of this protein is available. Crystal structures of SAM and TIR domains are available that are associated with some basic structural information of individual domains (Sporny et al., 2019). The crystal structures of ribose and $NADP^+$ complexes of SARM1 and plant NLR RUN1 TIR domains determine a conserved substrate binding site. Therefore, TIR domains mediated NAD^+ cleavage could be considered as a conserved feature of animal and plant cell death signalling pathways (Horsefield et al., 2019). In fact, a putative catalytic glutamic acid is conserved in both mammalian SARM1 NADase and bacterial TIR NADase (Wan et al., 2019). By phylogenetic analysis, it was shown that unlike other members (MyD88, TRIF, TRAM and MAL) of the TLR adaptor, SARM1 is closely related to bacterial TIR domain containing protein (Tcps). It suggests that SARM1 has a different evolutionary history from other animal TLR adaptors. SARM1 may have emerged via a lateral gene transfer from bacteria to animals. It was hypothesized that the bacterial TIR containing proteins may share the negative regulatory mechanism of TLR signalling to inhibit their eukaryotic host's immune response (Patterson and Werling, 2013; Zhang et al., 2011).

To compare the amino acid sequence similarities between TIR domain of SARM1 and other mammalian TLR adaptor proteins with bacterial TIR domain from *Brucella ovis* TIR containing protein B (TcpB), we created a multiple sequence alignment from sequences of TIR domain of human TLR adaptors and bacterial Tcps. Progressive pairwise alignments were generated, and we compared their percentage of

amino acid sequence similarity (Fig. 11 A-E). Interestingly, SARM1 TIR has comparatively higher (22%) amino acid sequence similarity with TIR domain of TcpB (Fig. 11 A), whereas, it is only 8%, 14%, 13% and 16% similar with TIR domain of TRAM, TRIF, MyD88 and MAL respectively (Fig. 11 B-E). This result is supporting the hypothesis that these two sequences may not arise independently, rather arose from a common ancestor.

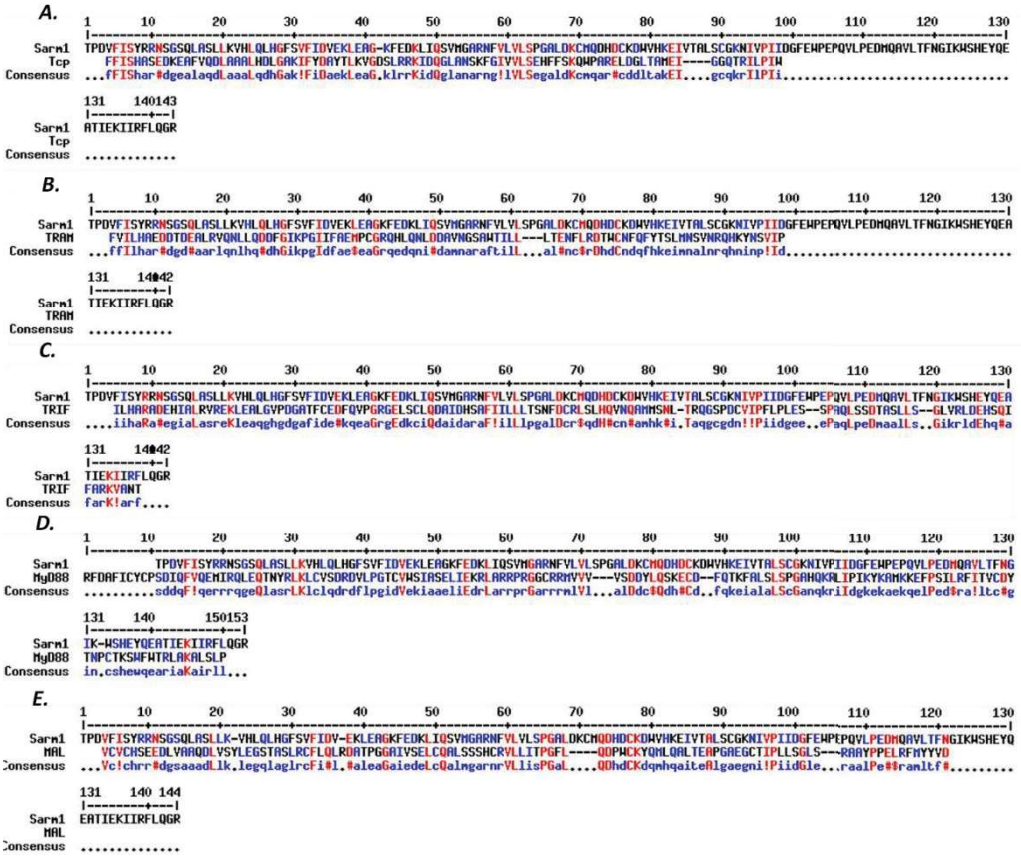

Fig. 11. Multalin comparison of SARM1 TIR with TIR domain of **(A)** Brucella ovis Tcp, **(B)** TRAM, **(C)** TRIF, **(D)** MyD88 and **(E)** MAL

It was also found that TIR domain of rest of the TLR adaptors other than SARM1 showed very less amino acid sequence similarities with TcpB TIR (Fig. 12 A-D).

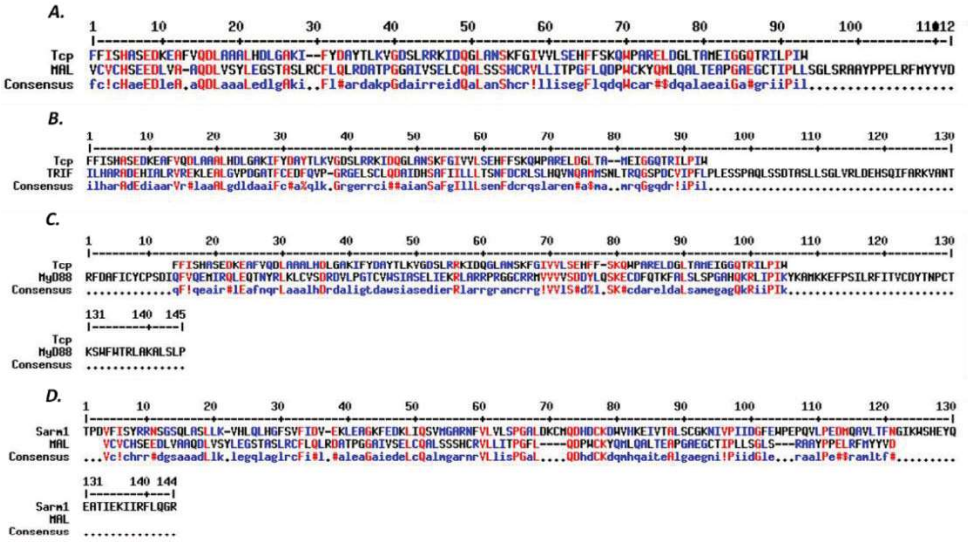

Fig. 12. Multalin comparison of TIR domain of *Brucella ovis* Tcp with **(A)** TRAM, **(B)** TRIF, **(C)** MyD88 and **(D)** MAL

We predicted secondary and tertiary structure of TIR domain from bacterial Tcps and human SARM1 and found similar secondary structures in both TIR domain of bacterial Tcps and human SARM1 (Fig. 13 A, B). TIR domains from both showed higher percentages of alpha helix. To compare this specific domain with other TIR containing TLR adaptors, we also predicted secondary structures of MyD88, TRAM, MAL and TRIF by using the same software (Fig. 13 C-F). But, unlike TIR domain of SARM1, we did not find any such similar secondary structures in TIR domains of these adaptors that showed comparative lower alpha helical structures.

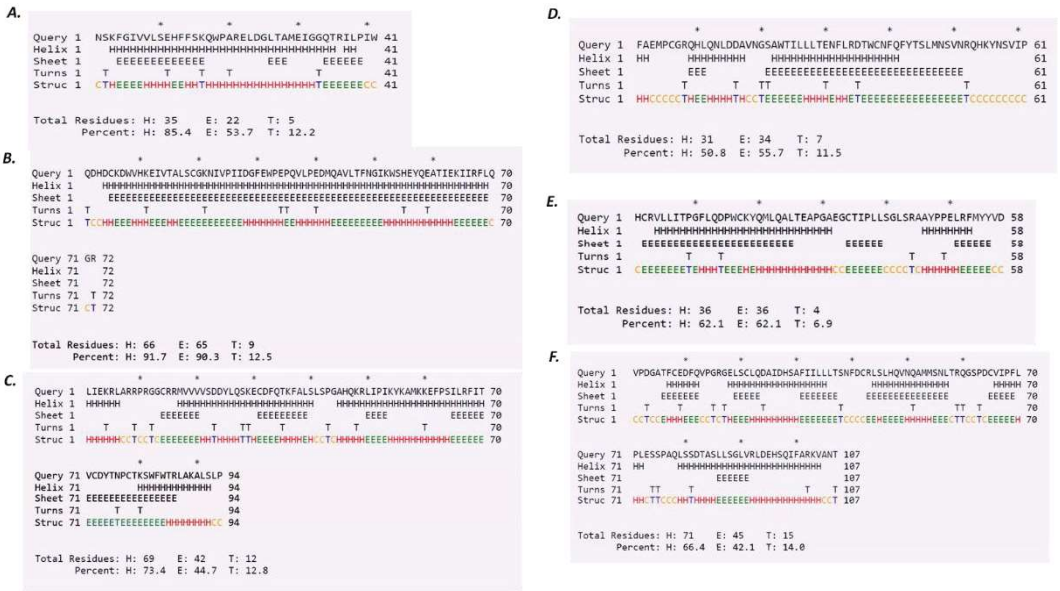

Fig. 13. Secondary structure prediction of TIR domain of **(A)** Tcp, **(B)** SARM1, **(C)** MyD88, **(D)** TRAM, **(E)** MAL and **(F)** TRIF

Template based tertiary structure prediction of TIR domain of SARM1 showed similarity with the TIR domain of the immunosuppressor TcpB from *Brucella ovis*, with 99.9% confidence (Fig.14 A). Whereas other TIR containing TLR adaptors are not found to be associated with such similar tertiary structures, MyD88, TRAM, MAL and TRIF are structurally similar with human toll like receptor 5 with 100% confidence, TIR domain containing adaptor molecule 2 with 99.9% confidence, human toll like receptor 5 with 99.9% confidence and TIR domain containing adaptor molecule 1 with 99.9% confidence respectively (Fig.14 B-E). These results suggest that among all five TIR domain containing TLR adaptor proteins, SARM1 has unique and very high structural similarities with bacterial TIR containing proteins. Also, TcpB TIR shares the NADase activity like SARM1 (Wan et al., 2019). Combining, the claim of SARM1 having a prokaryotic origin is strengthened by this analysis.

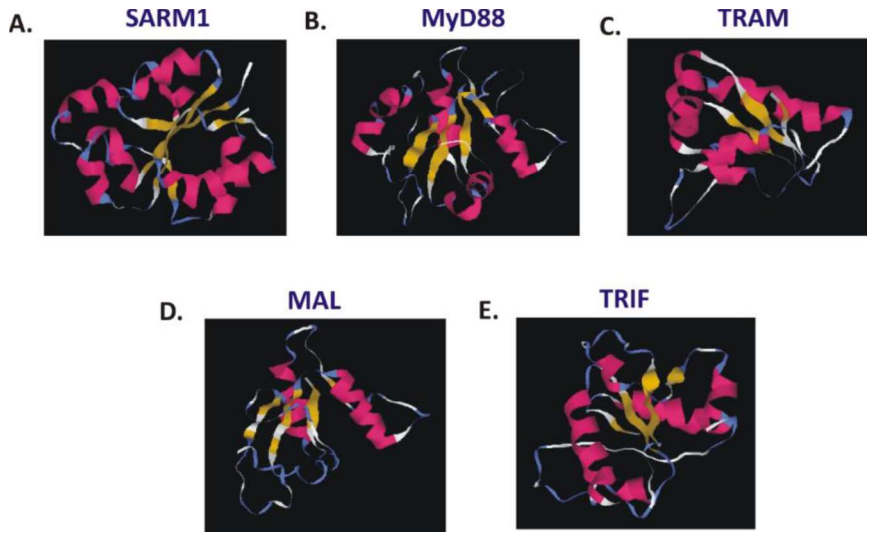

Fig. 14. Tertiary structure prediction of TIR domain of **(A)** SARM1, **(B)** MyD88, **(C)** TRAM, **(D)** MAL and **(E)** TRIF

1.3.1.3 SAM domain of human SARM1 may bind macromolecules like DNA or RNA and it possesses nuclear export signal (NES)

It has been reported that by using its amino-terminal ARM domain, SARM1 translocate to the nucleus in human embryonic kidney cells. Within the nucleus, it forms a lattice akin to the nuclear lamina scaffold. SARM1 also protects lamins from apoptotic degradation. Proinflammatory cytokine TNFα mediated signalling results in inter nucleosomal DNA fragmentation, that is also reduced by SARM1 translocation (Sethman and Hawiger, 2013). SARM1 was found to be critical for the recruitment of

RNA polymerase II and transcription factors to the *Ccl5* promoter in macrophages (Gürtler et al., 2014). However, no experimental evidence was provided till date for DNA/RNA binding site of SARM1. In order to determine whether SARM1 has any DNA/RNA binding site, we analysed its sequence information by using proNA and found that SAM domain of this protein consists of a nucleotide binding site that can bind DNA/RNA (Fig. 15).

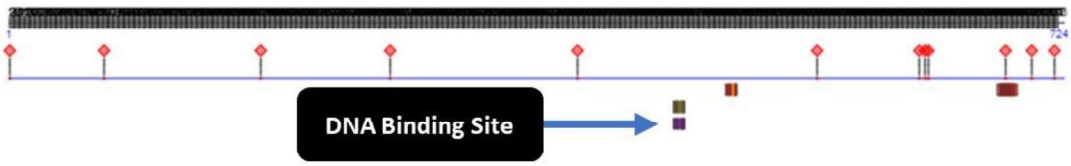

Fig. 15. Prediction of DNA binding site in SARM1 protein sequence as shown by proNA

As SARM1 was found to be associated with DNA binding site, and it was reported to translocate in nucleus (Sethman and Hawiger, 2013), we were curious to know whether it also has nuclear export signal (NES). Interestingly, we found that nine amino acids (a-a 75-83) have potential to export from nucleus, as they carry NES (Fig. 16). However, the function of this NES in SARM1 is not yet known and remains to be explored further.

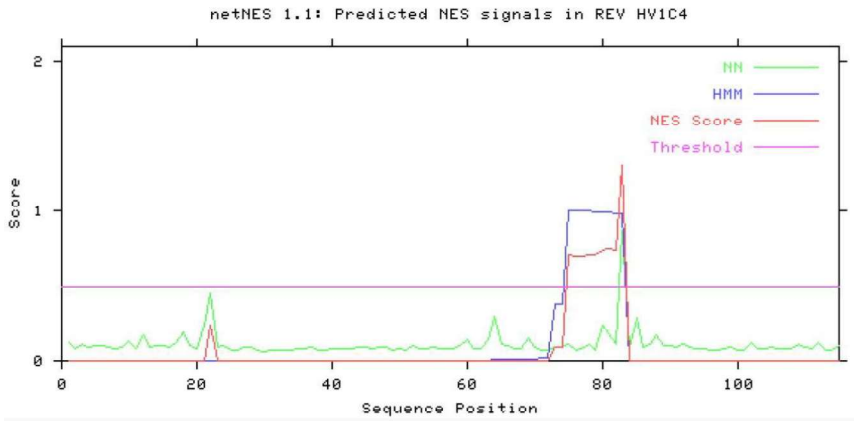

Fig. 16. Prediction of nuclear export signal (NES) in SARM1 protein sequence as shown by NetNES 1.1 online server

1.3.2 Evaluating the role of endogenous SARM1 in mitochondrial homeostasis

1.3.2.1 The mitochondrial complex I inhibitor rotenone induces cell death in a dose and time-dependent manner in SH-SY5Y cells

To understand the role of endogenous SARM1, we treated SH-SY5Y cells with the mitochondrial complex I inhibitor rotenone. Since previous studies have

indicated that SARM1 localizes to the mitochondria upon stress and induce axonal retraction (Mukherjee et al., 2013; Murata et al., 2013) we chose the mitochondrial complex I inhibitor rotenone as our treatment of choice. The neuroblastoma cell line SH-SY5Y has several characteristics of dopaminergic neurons (Xie et al., 2010) and hence treatment with rotenone, which has been implicated in sporadic cases of PD, could help us understand whether SARM1 also played a role in dopaminergic neuronal loss as often seen in PD. SH-SY5Y cells were treated with 2.5 and 5 µM of rotenone for 24 h and 48 h. Cells showed signs of neurite retraction at 24 h post treatment as evident by staining with Tubulin without any damage to the cell body (Fig. 17 A, B). Cell death following rotenone treatment was more prominent at 48 h post treatment (Fig. 17 C). Hence, we envisioned that rotenone treatment to SH-SY5Y cells at 24 h post treatment could serve as an excellent *in vitro* model of studying degeneration of neuronal projections, a hallmark of several neurodegenerative diseases like Parkinson's disease and the role of SARM1 in the process.

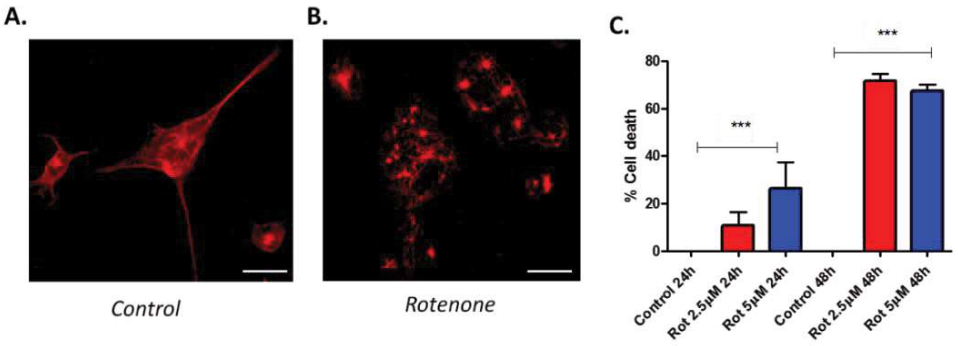

Fig. 17. Rotenone treatment in SH-SY5Y cells **(A, B)** Immunofluorescence analysis of SH-SY5Y cells treated with 5 µM of rotenone for 24 h **(B)** and compared to untreated control cells **(A)**. Tubulin staining of both the treated and untreated samples are shown. Scale bars = 10 µm **(C)** MTT assay of SH-SY5Y cells treated with rotenone (2.5 and 5 µM) for 24 and 48 h. Results are representative of at least five independent experiments. *p < 0.05, **p < 0.01, and ***p<0.001 compared to control sample

1.3.2.2 Rotenone treatment results in mitochondrial damage in SH-SY5Y cells

Since rotenone is a mitochondrial complex I inhibitor and known to affect mitochondrial respiration (Won et al., 2015) we sought to determine whether rotenone treatment at the doses describes previously affected mitochondrial homeostasis. To determine whether rotenone causes mitochondrial damage in SH-SY5Y cells, cells were treated with 5 µM of rotenone for 24 h and labelled with MitoTracker Green, a fluorescent dye that stains mitochondria. Fluorescence microscopy revealed that

rotenone treated cells were associated with reduction of mitochondrial puncta, compared to control cells (Fig. 18 A). Apart from neuronal cell population, SARM1 has also been found to express in kidney cells. To further confirm the effect of rotenone on mitochondrial homeostasis, mitochondrial membrane potential using TMRM dye was determined in HEK293 cells, a non-neuronal cell but known to express endogenous SARM1 (Fig. 18 B). Our results indicate that rotenone treatment causes loss of mitochondrial membrane potential with subsequent accumulation of damaged mitochondria as evident by loss of puncta structure and increased intensity of mitotracker green dye following rotenone treatment.

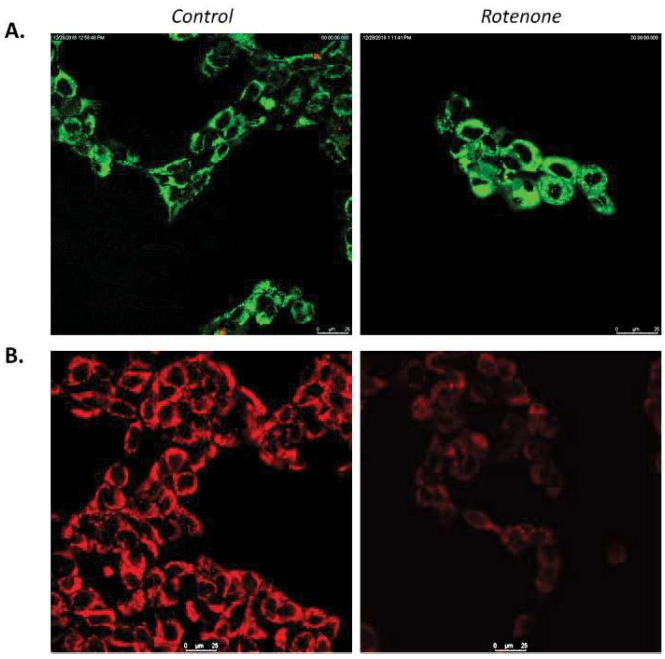

Fig. 18. Rotenone treatment in SH-SY5Y and HEK293 cells; **(A)** labelling of mitochondria using MitoTracker Green in SH-SY5Y cells showed a reduction in rotenone treated cells, compared to control **(B)** HEK293 cells treated with TMRM dye showed a reduction in mitochondrial potential in rotenone treated cells, compared to control. Scale bars = 10 µm

1.3.2.3 Rotenone treatment induces *Sarm1* expression and is required for rotenone induced cell death in SH-SY5Y cells

It has been previously found that in sensory neurons, rotenone induces SARM1 dependent cell death and axonal degeneration (Summers et al., 2014). To understand whether rotenone treatment of SH-SY5Y cells results in SARM1 induction, *Sarm1* gene expression was analysed at 24 h post treatment and was found to be significantly increased in the cells following rotenone treatment (Fig. 19 A). Since SARM1 was previously shown to localize to the mitochondria upon stress

(Mukherjee et al., 2013; Murata et al., 2013) we assessed SARM1 localization in both the nuclear and mitochondrial fraction. We observed SARM1 localization both at the nuclear and mitochondria with more prominent localization at the mitochondria (Fig. 19 B) indicating that SARM1 may mediate mitochondrial dysfunction following rotenone treatment.

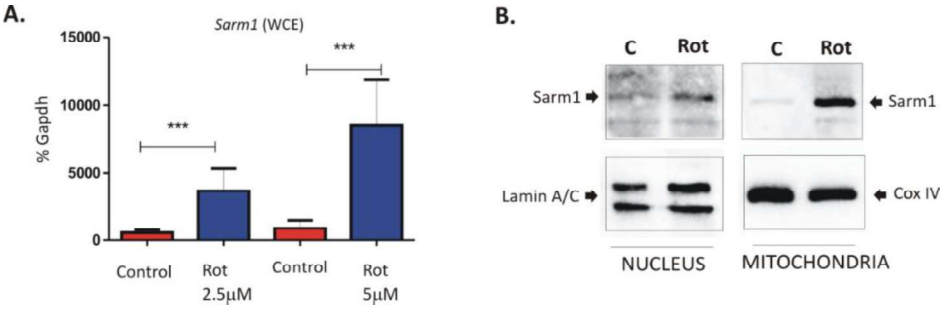

Fig. 19. Real time PCR analysis of SH-SY5Y cells treated with 2.5 and 5μM of rotenone for 24 h **(A)** Expression of *Sarm1* from whole cell extracts. **(B)** Analysis of SARM1 protein levels in the nuclear and mitochondrial fractions of rotenone (5μM) treated SH-SY5Y cells. Lamin and COX IV were used as loading control for the nuclear and mitochondrial fraction respectively. Results are representative of at least three independent experiments. *p < 0.05, **p < 0.01, and ***p<0.001 compared to control sample

To test whether SARM1 was required for rotenone induced cell death, cells were transfected with siSARM1 for 24 h. Our results indicate that prior treatment with siRNA for SARM1 followed by 5 μM of rotenone treatment significantly reversed cell death (Fig. 20 A) and SARM1 protein levels were also reduced in these cells (Fig. 20 B) indicating that SARM1 is the key mediator of the rotenone induced neurotoxicity in SH-SY5Y cells.

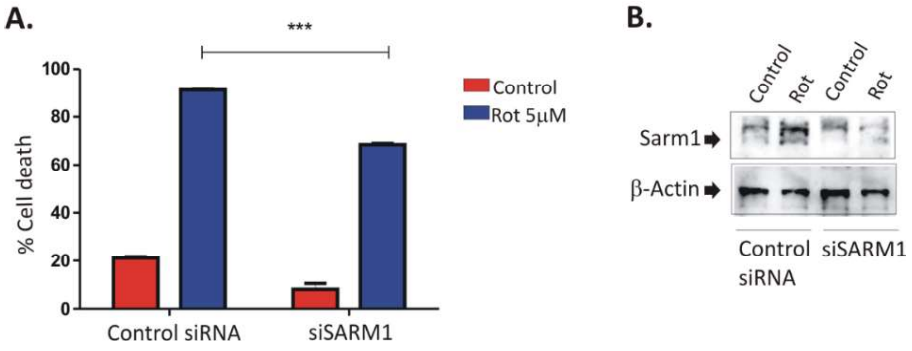

Fig. 20. SH-SY5Y cells were treated with 25 nM of SARM1 siRNA or control (nontargeting) siRNA for 24 h followed by 5 μM of rotenone treatment for 24 h. **(A)** MTT assay of cells treated with rotenone in the presence or absence of siRNAs was performed. **(B)** Analysis of SARM1 protein levels in the whole cell extracts of cells transfected with SARM1 or control siRNA in the presence or absence of rotenone (5 μM). β-actin was used as a loading control.

Results are representative of at least three independent experiments. *p < 0.05, **p < 0.01, and ***p<0.001 compared to control sample

1.3.2.4 Rotenone treatment results in de-regulation of ETC complex genes in SH-SY5Y cells

It has been already reported that rotenone impairs mitochondrial electron transport chain (Won et al., 2015). However, the effect of rotenone in ETC complex gene expression is not well understood yet. Further, SARM1 has been shown to interact with the mitochondrial protein ATP synthase. To evaluate the effect of rotenone treatment on the expression of the ETC complex genes and the role of SARM1, the expression of several genes of mitochondrial complex I, complex III, complex IV and complex V were analysed in the whole cell extracts after 24 h treatment with rotenone. Rotenone treatment resulted in the deregulation of several ETC complex genes with significant increase in the expression of *Ndufs2*, *Cox5B* and *Atp12A* which are nuclear encoded (Fig. 21).

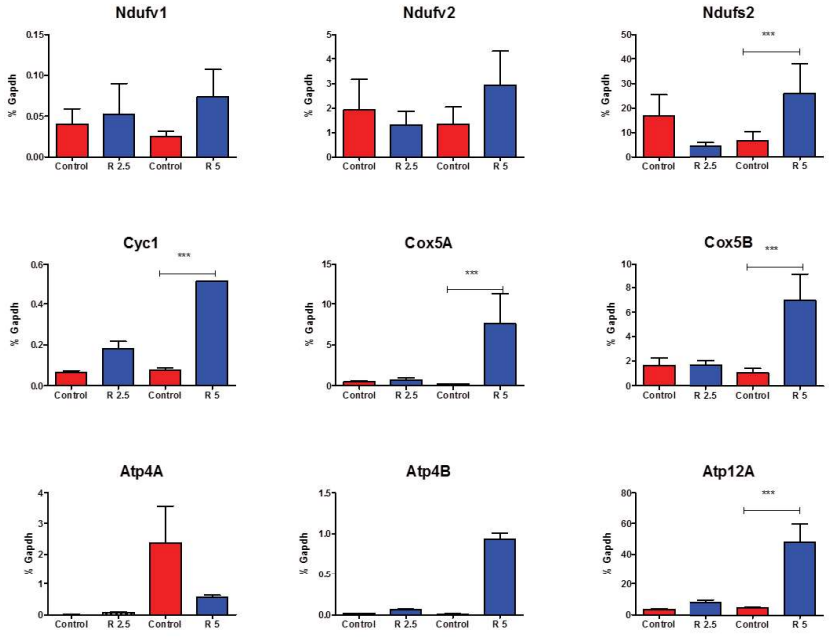

Fig. 21. Real-time PCR analysis of SH-SY5Y cells treated with 2.5 and 5 µM of rotenone for 24 h. Expression of ETC complex genes from whole cell extracts were analysed. Results are representative of at least three independent experiments. *p < 0.05, **p < 0.01, and ***p<0.001 compared to control samples

In order to determine whether SARM1 played a role in rotenone mediated de-regulation of ETC complex genes, SH-SY5Y cells were transfected with siSARM1. Our results indicate that prior treatment with siRNA for SARM1 for 24 h followed by

5 µM of rotenone treatment significantly reversed rotenone mediated de-regulation of ETC complex genes (Fig. 22 A, B) suggesting that SARM1 may play a role in the regulation of nuclear ETC complex gene expression via direct or indirect mechanism.

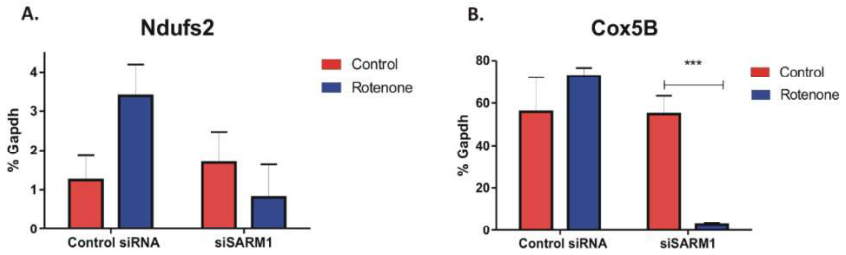

Fig. 22. Real-time PCR analysis of SH-SY5Y cells treated with 25 nM of SARM1 siRNA or control (nontargeting) siRNA for 24 h followed by 5 µM of rotenone treatment for 24 h. **(A, B)** Expression of ETC complex genes from whole cell extracts were analysed. Results are representative of at least three independent experiments. *p < 0.05, **p < 0.01, and ***p<0.001 compared to control samples

1.3.2.5 Rotenone mediated cell death and SARM1 induction is reversed in the presence of NR, a precursor of NAD^+

Recent studies have shown that the TIR domain of SARM1 has intrinsic NADase activity that may cause gross energy deficit within the cells ultimately leading to neurodegeneration (Essuman et al., 2017). It has been found that aging mice fed with the NAD^+ precursor nicotinamide riboside (NR) were protected from muscle degeneration (Zhang et al., 2016). To determine the NAD^+ levels in rotenone treated cells, SH-SY5Y cells were treated with 5 µM of rotenone for 24 h and NAD^+ levels were analysed. We observed a significant reduction of NAD^+ levels in rotenone treated cells (Fig. 23 A), indicating that rotenone mediated SARM1 upregulation may have a direct role in the reduction of cellular NAD^+ levels and induction of subsequent cell death. To further determine whether SARM1 mediated axon degeneration could be blocked by the external supply of NR, SH-SY5Y cells were treated with NR (0.5 mM) along with rotenone (5 µM) to check the effect of NR in SARM1-mediated cell death following rotenone treatment. A significant reversal of rotenone mediated cell death was observed (Fig. 23 B) along with the reduction in *Sarm1* gene expression (Fig. 23 C), indicating that NAD^+ levels may play a role in SARM1 mediated cell death and this effect could be partially reversed in the presence of NAD^+ precursor nicotinamide riboside.

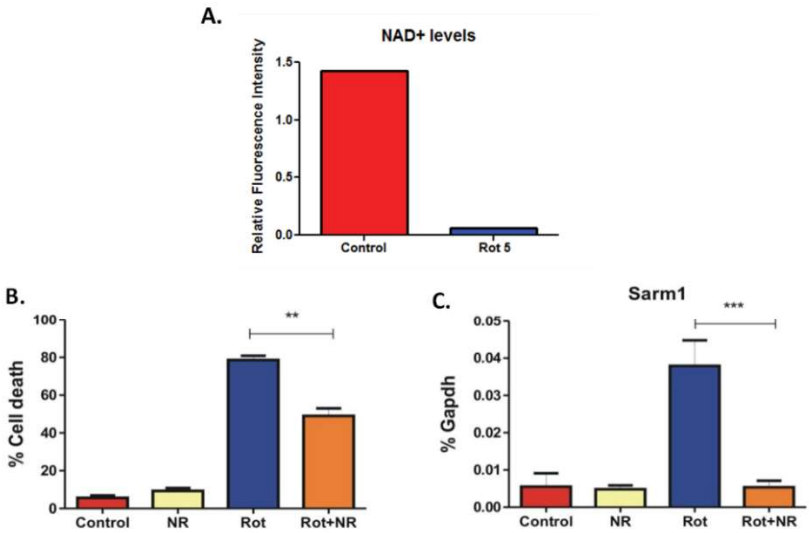

Fig. 23. SH-SY5Y cells were treated with rotenone along with NR. **(A)** NAD^+ levels detection assay of SH-SY5Y cells treated with 5 µM of rotenone for 24 h. **(B)** MTT assay of cells treated with rotenone (5 µM) and NR (0.5 mM) for 24 h. **(C)** Real-time PCR analysis of SH-SY5Y cells treated with rotenone (5 µM) and NR (0.5 mM) for 24 h. Expression of Sarm1 from whole cell extracts was analysed. Results are representative of at least three independent experiments. *p < 0.05, **p < 0.01, and ***p<0.001 compared to control sample

1.3.2.6 Rotenone induced de-regulation of the respiratory complex genes is partially reversed in the presence of NR

In our previous experiment, it was found that NR could reverse the rotenone mediated cell death and Sarm1 expression. Therefore, to determine whether rotenone induced de-regulation of ETC complex genes is also reversed in NR treated cells, SH-SY5Y cells were treated with 0.5 mM of NR along with 5 µM of rotenone for 24 h. Although there was not much change in the expression levels of *Ndufs2* gene, the expression of *Cox5B* and *Atp12a* was significantly reduced following NR treatment (Fig. 24 A-C). Our findings suggest that external supply of NR could replenish NAD^+ levels in rotenone treated cells and reduce stress induced *Sarm1* upregulation that could further reverse de-regulation of ETC complex gene expression in SH-SY5Y cells.

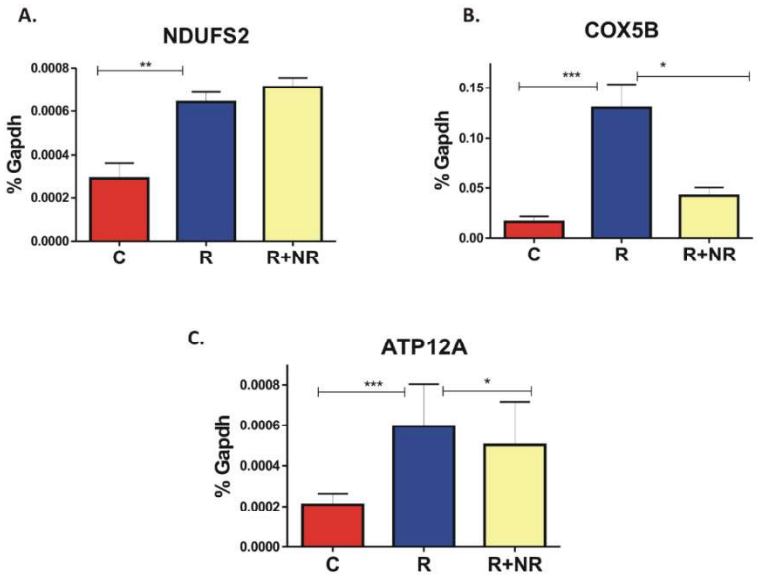

Fig. 24. Real-time PCR analysis of SH-SY5Y cells treated with rotenone (5 µM) and NR (0.5 mM) for 24 h. Expression of ETC complex genes from whole cell extracts were analysed. Results are representative of at least three independent experiments. *p < 0.05, **p < 0.01, and ***p<0.001 compared to control sample

1.3.2.7 Rotenone increases *Sirtuin* gene expression that is reversed in NR treated cells

It has been reported that in a model of amyotrophic lateral sclerosis overexpression of SIRT1 protected against neurodegeneration that was induced by a mutant form of superoxide dismutase (Gan and Mucke, 2008). Sirtuin requires NAD^+ as a cofactor unlike other deacetylases (Chalkiadaki and Guarente, 2012; Zhang et al., 2009). Since the NAD^+ precursor NR reversed the deregulation of ETC complex genes induced by rotenone, we speculated that NAD^+ levels may have a role on the mitochondrial Sirtuins that uses NAD^+ as a co-factor. Further, a few reports suggest that Sirtuins may play an important role in the deacetylation of the ETC complex genes and thus regulated their activity (Nogueiras et al., 2012). We observed a significant upregulation of the expression of *Sirtuin* genes that was reversed in the presence of NR (Fig. 25), indicating that NR treatment reduces rotenone mediated heightened expression of *Sirtuins* that may play an important role in the regulation of mitochondrial homeostasis.

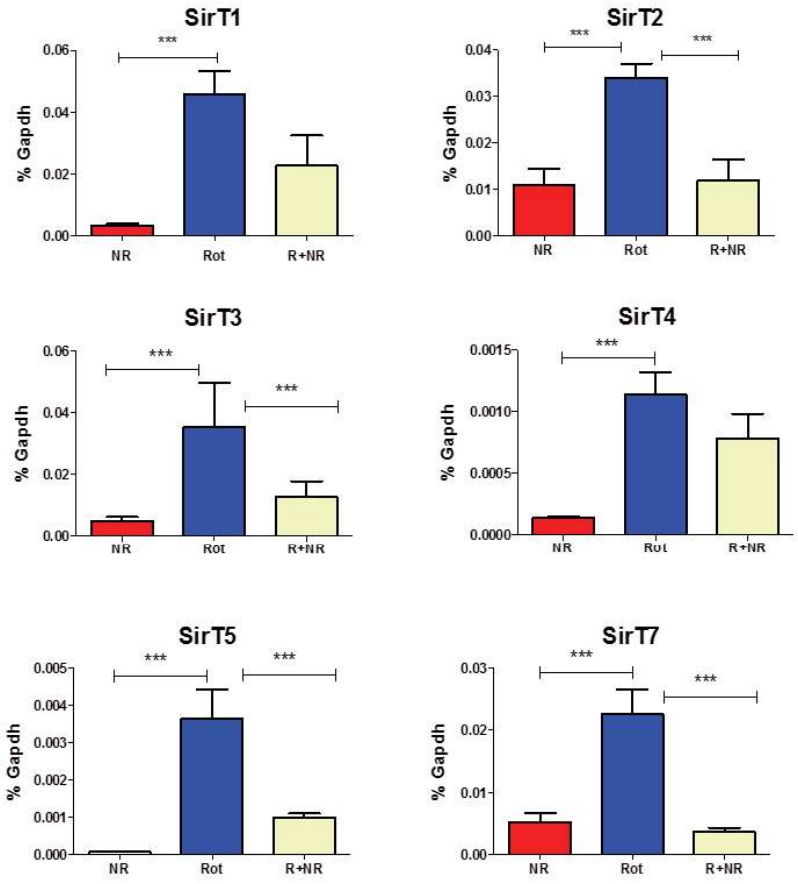

Fig. 25. Real-time PCR analysis of SH-SY5Y cells treated with rotenone (5 µM) and NR (0.5 mM) for 24 h. Expression of *Sirtuin* genes from whole cell extracts were analysed. Results are representative of at least three independent experiments. *p < 0.05, **p < 0.01, and ***p<0.001 compared to control sample

1.3.2.8 Rotenone induced cell death and SARM1 induction is partially reversed in the presence of calcium channel blockers

It has been shown that SARM1 functions downstream of the axonal calcium increases after axotomy, as in *C. elegans* tir-1 (homolog of human SARM1) acts downstream of the Ca^{2+}-CaM kinase signalling pathway (Chang et al., 2011; Chuang and Bargmann, 2005). In order to understand whether the calcium acts upstream of SARM1 induction and plays a major role in SARM1 mediated cell death, SH-SY5Y cells were treated with 10 µM of nimodipine (calcium channel blocker) along with 5 µM of rotenone and a delayed cell death along with a significant reversal of the rotenone induced *Sarm1* expression was observed following nimodipine treatment (Fig. 26 A, B).

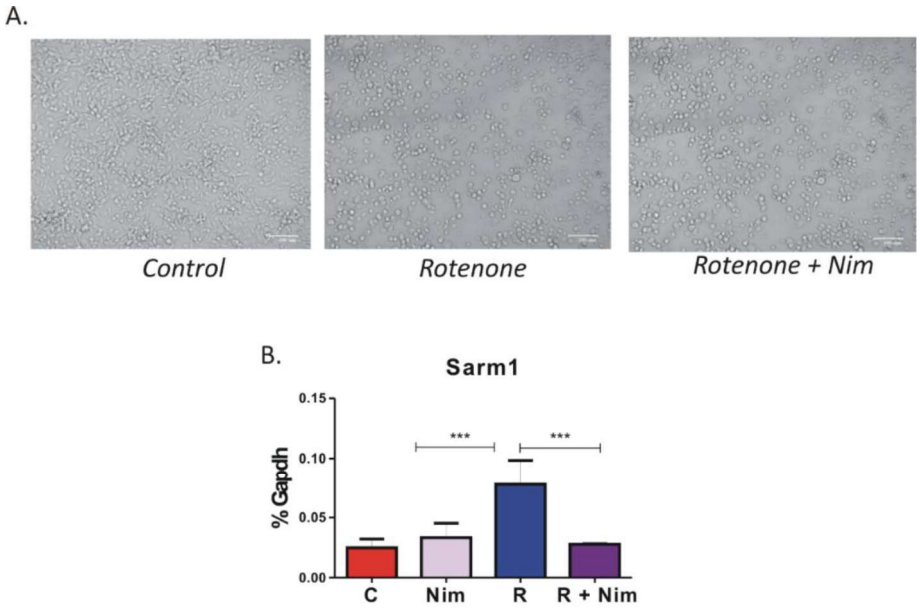

Fig. 26. SH-SY5Y cells were treated with rotenone along with nimodipine. **(A)** Axonal retraction of SH-SY5Y cells treated with 5 µM of rotenone and 10 µM of nimodipine for 24 h. **(B)** Real-time PCR analysis of SH-SY5Y cells treated with rotenone (5 µM) and nimodipine (10 µM) for 24 h. Expression of *Sarm1* from whole cell extracts was analysed. Results are representative of at least three independent experiments. *p < 0.05, **p < 0.01, and ***p<0.001 compared to control sample

It has been previously found that EGTA suppresses axon degeneration upon CCCP treatment, which determines that Calcium influx is required for neurodegeneration during mitochondrial dysfunction (Daniel W Summers et al., 2014). To further confirm the role of calcium rotenone induced neurodegeneration, the calcium ion chelator EGTA (2.5 mM) was added in the presence or absence of rotenone. As observed previously a significant reversal of the *Sarm1* expression was found along with a delayed rotenone induced cell death (Fig. 27 A, B), suggesting that calcium may play a role in SARM1 mediated cell death.

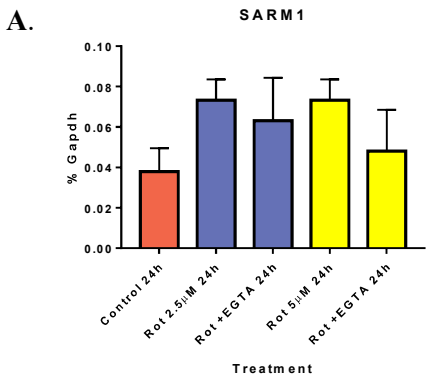

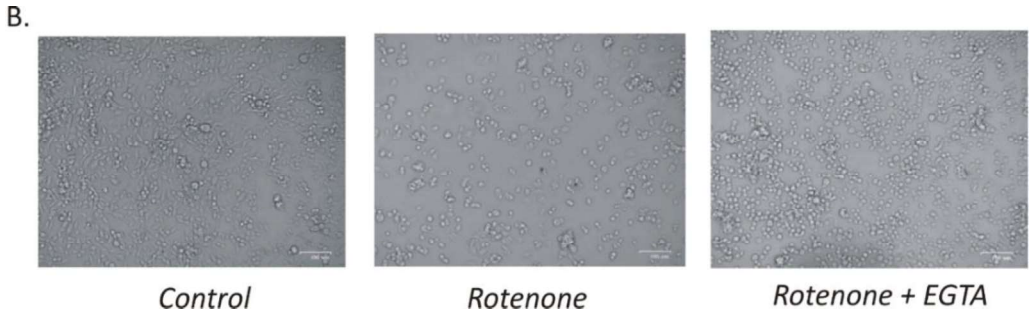

Fig. 27. SH-SY5Y cells were treated with rotenone along with EGTA. **(A)** Real-time PCR analysis of SH-SY5Y cells treated with rotenone (5 µM) and EGTA (2.5 mM) for 24 h. Expression of *Sarm1* from whole cell extracts was analysed. **(B)** Axonal retraction of SH-SY5Y cells treated with 5 µM of rotenone and 2.5 mM of EGTA for 24 h. Results are representative of at least three independent experiments. *p < 0.05, **p < 0.01, and ***p<0.001 compared to control sample

1.3.2.9 Rotenone induced de-regulation of the respiratory complex genes is partially reversed in the presence of nimodipine

In our previous experiment, it was found that nimodipine could reverse the rotenone mediated cell death and *Sarm1* expression. Therefore, to determine whether rotenone induced de-regulation of ETC complex genes is also reversed in nimodipine treated cells, SH-SY5Y cells were treated with 10 µM of nimodipine along with 5 µM of rotenone for 24 h and a significant reversal of de-regulation of ETC complex gene expression was observed following nimodipine treatment (Fig. 28). Our findings suggest that blocking of Calcium elevation causes reduction of *Sarm1* expression that further reverses de-regulation of ETC complex gene expression, indicating that *Sarm1* expression may have correlation with these ETC complex genes.

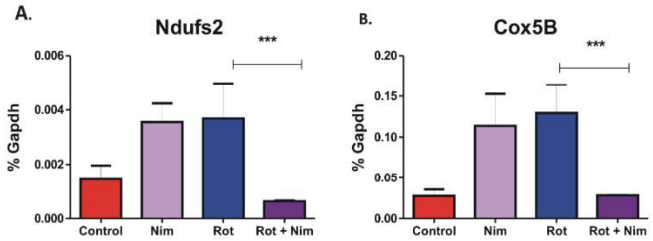

Fig. 28. Real-time PCR analysis of SH-SY5Y cells treated with rotenone (5 µM) and nimodipine (10 µM) for 24 h. Expression of ETC complex genes from whole cell extracts was analysed. Results are representative of at least three independent experiments. *p < 0.05, **p < 0.01, and ***p<0.001 compared to control sample

1.3.3 SARM1 overexpression studies in SH-SY5Y and HEK293 cells

1.3.3.1 Overexpression of SARM1 and its mutants leads to cell death in SH-SY5Y cells

It has been shown previously that SARM1 is an essential mediator of axon degeneration (Lewis, 2015) that requires both SAM and TIR interactions (J. Gerdts et al., 2013) to execute such function. In order to identify the major domain that acts in this neurodegeneration, several deletion mutants of SARM1 were generated (Fig. 29) as described in the methodology section (vide Section 1.2.2.1).

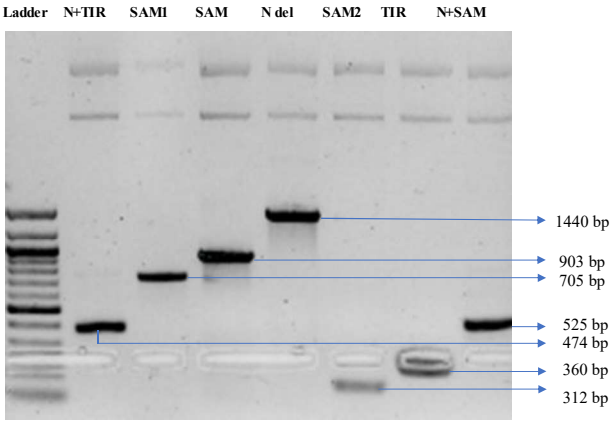

Fig. 29. Deletion mutants of SARM1 cloned in pCMV6 vector. Vectors were digested by restriction endonucleases (EcoRI and XhoI) and base pair length of each SARM1 mutants were compared with the respective ladder size

Overexpression of SARM1 gene and its eight deletion mutants in the SH-SY5Y cells by transient transfection resulted in retraction of neurite projection at 24 h post treatment without any damage in the cell body (Fig. 30 A). A significant cell death at 48 h post treatment was also found in these cells (Fig. 30 B). Among them, TIR domain was found to play the most essential role in this neurodegeneration with or without N-terminal peptide moiety, followed by SAM domain, indicating that the TIR domain of SARM1 act as executioner of neurodegeneration and correlates with its evolutionary distinct nature as predicted by our *in silico* analysis.

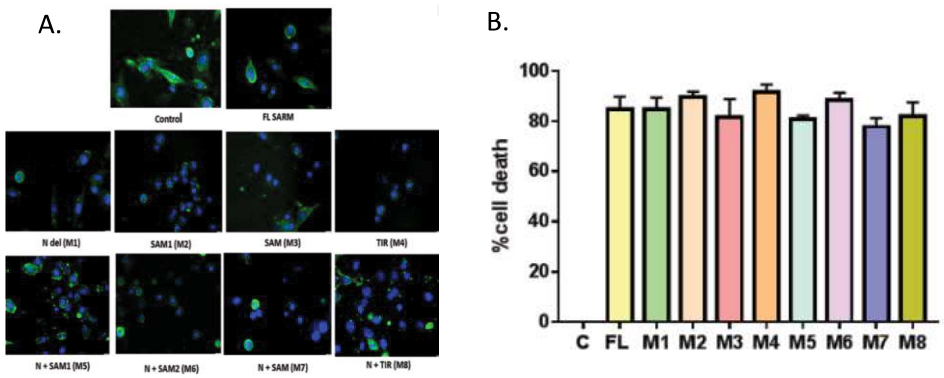

Fig. 30. SH-SY5Y cells were overexpressed with SARM1 **(A)** Immunofluorescence analysis of SH-SY5Y cells overexpressed with different SARM1 deletion mutants for 24 h and compared to non-transfected control cells. DAPI (blue) and MAP2 (green) staining of both the transfected and non-transfected samples are shown. **(B)** MTT assay of cells overexpressed with different SARM1 deletion mutants for 48 h was performed. Results are representative of at least three independent experiments. *p < 0.05, **p < 0.01, and ***p<0.001 compared to control samples

1.3.3.2 Overexpression of SARM1 and its mutants results in de-regulation of ETC complex genes distinct from endogenous SARM1

To understand the effect of SARM1 and its different deletion mutants on the expression of the ETC complex genes, the expression of several genes of mitochondrial complex I, complex III, complex IV and complex V were analysed in the SARM1 overexpressed cells. Overexpression of SARM1 and its different deletion mutants resulted in the deregulation of several ETC complex genes (Fig. 31). Interestingly, expression of these genes was differentially de-regulated as compared to rotenone treatment, indicating that endogenous expression of SARM1 that was caused by rotenone treatment may play a unique role in regulation of ETC complex gene expression than that in SARM1 overexpressed cells.

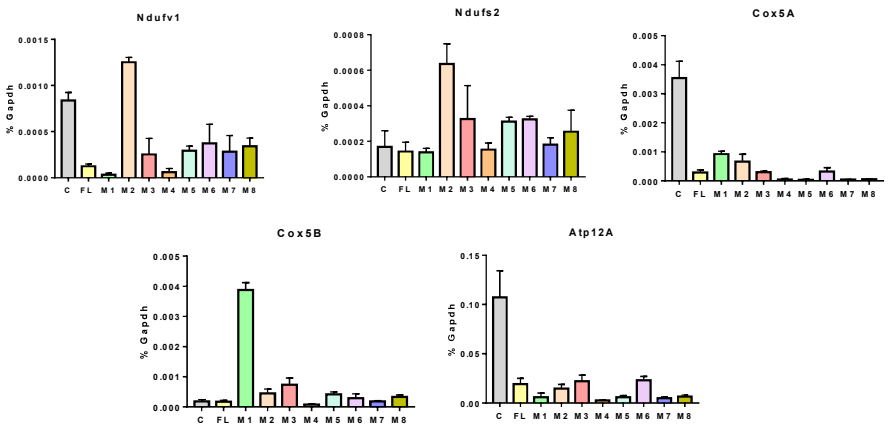

Fig. 31. Real-time PCR analysis of SH-SY5Y cells overexpressed with different SARM1 deletion mutants and non-transfected cells. Expression of ETC complex genes from whole cell extracts were analysed. Results are representative of at least three independent experiments. *p < 0.05, **p < 0.01, and ***p<0.001 compared to control samples

1.4 Discussion

TIR domain of human SARM1 is sequentially and structurally similar to TIR domain of bacterial Tcp than the other four mammalian TIR containing TLR adaptors (TRAM, TRIF, MyD88 and MAL), whereas these four adaptors have very less sequence similarity with TIR domain of Tcp. It can be hypothesized from this finding that SARM1 and Tcp did not arise independently, rather have arisen from a common ancestor. Interestingly, when the domain of human SARM1 was compared with *C. elegans* tir-1 (homolog of mammalian SARM1), there was more dissimilarity at the TIR domain which could explain the difference in the function of these two proteins. Further, as discussed earlier, the TIR domain of SARM1 is more closely related with bacterial TIR containing proteins which also possess an intrinsic NADase activity. A recent publication has also shown that human SARM1 is more closely related to plant TIR-containing proteins that have an important role in the innate immune function within the plants (Wan et al., 2019). Thus, our *in silico* analysis point towards the important function of SARM1 TIR domain and how it may play an important role in mediating energy deficit within the cells through its NADase activity.

To perform an in-depth mechanistic analysis of SARM1 function, our aim was to set up an *in vitro* cellular model system that could be used to study the function of endogenous SARM1. For this, we used the mitochondrial complex I inhibitor rotenone for our assays. Rotenone treatment of SH-SY5Y cells results in neurite

retraction, SARM1 induction and its localization to the mitochondria. Further, using knock down assays SARM1 was shown for the first time to be required for rotenone induced cell death.

In a previous study SARM1 was shown to induce ROS following virus infection (Mukherjee et al., 2013). Here we speculated that SARM1 might play a role in rotenone mediated ROS generation. Further, SARM1 was also shown to interact with the mitochondrial ATP synthase, the impact of which is poorly understood. Regulation of mitochondrial electron transport chain (ETC) activity in various cellular stress conditions plays an important role in ROS production and deregulation of these complexes may lead to over production of mitochondrial ROS. Alteration of ETC activities may also lead to poor progression of cellular respiration that may result in mitochondrial reactive oxygen species (ROS) generation and eventually damage mitochondria and induce cell death. Our results indicate that rotenone treatment induces loss of mitochondrial membrane potential along with the deregulation of the ETC complex genes. Interestingly, the levels of *Ndufs2*, *CoxVB* and *ATP12A* genes were significantly upregulated following rotenone treatment. Rotenone treatment also reduces NAD^+ levels in cells causing a gross energy deficit that correlate with the increased SARM1 expression. Importantly, pre-incubation with the NAD^+ precursor nicotinamide riboside reverses rotenone induced cell death and also reduces *SARM1* gene expression. This is also accompanied by a marked reduction in *Ndufs2*, *CoxVB* and *ATP12A* gene expression. *Ndufs2* serves as the point of entry in complex I and it is interesting to speculate that it might directly correlate with mitochondrial complex I deficiency arising from rotenone treatment in these cells.

Mitochondrion is one of the intracellular stores for calcium and since rotenone treatment results in mitochondrial depolarization, we wanted to study the effect of the calcium channel blocker nimodipine and the calcium chelator EGTA on the effect of *SARM1* and ETC complex genes following rotenone treatment. Pre-incubation with the calcium channel blocker nimodipine partially reverses rotenone induced cell death and reduces *SARM1* and the ETC gene expression. Since rotenone treatment was associated with reduced NAD^+ levels, we wanted to check whether besides the NADase SARM1, other NAD^+ consuming enzymes like Sirtuins play a role in rotenone mediated neurotoxicity. Interestingly, both NR and nimodipine treatment reduces the heightened expression of *Sirtuins* that may play an important role in the

regulation of mitochondrial homeostasis, the mechanism of which needs to be explored further.

Overexpression of SARM1 and its different mutants in SH-SY5Y cells induced neurite retraction and ultimately cell death. Cell death was more prominently induced by the TIR domain of SARM1 pointing again to its important role in cell death. However, the deregulation of ETC complex genes was not similar in rotenone induced celled death vs in SARM1 overexpressed cells. This indicate that rotenone mediated induction of SARM1 alters its activity in a manner distinct from overexpressed SARM1 which emphasizes the importance of rotenone treated cell lines as a good surrogate model to study SARM1 function in regulation of mitochondrial homeostasis and cell death networks.